Part I
MOF Chemistry of Metallic Clusters and Other Nodes

The Chemistry of Metal–Organic Frameworks: Synthesis, Characterization, and Applications, First Edition.
Edited by Stefan Kaskel.

3
Reticular Chemistry of Metal–Organic Frameworks Composed of Copper and Zinc Metal Oxide Secondary Building Units as Nodes

Alexander Schoedel and Omar M. Yaghi

3.1
Introduction

Metal–organic frameworks (MOFs) have attracted enormous scientific interest over the past two decades due to their high crystallinity, exceptional porosity, high modularity, and diverse functionality [1]. The opportunity to achieve functional materials by design with promising properties, unattainable for solid-state materials in general, distinguishes MOFs from any other class of materials, in particular, traditional porous materials, for example, zeolites [2], mesoporous silica [3], and porous carbon [4]. Concepts such as the node and spacer principle [5] are based on simple geometrical analysis, which is facilitated by direct joining of polyhedral or polygonal nodes and linkers to translate their geometry into nets with predictable topology and structure. The obtained crystalline materials represent well-defined structures that allow for studying the design, synthesis, and properties of materials by means of single-crystal X-ray diffraction. Herein, we introduce the concept of secondary building units (SBUs) [1a] as a critical design element for the synthesis of rigid, permanently porous MOFs. Furthermore, the cluster chemistry of copper and zinc is highlighted due to the depth and diversity of their SBU geometries, which allow them to be used in linking with organic units (reticular chemistry) [6]. These will be introduced and exemplified by prominent MOF structures, demonstrating net topologies that have produced numerous functional and expanded frameworks.

3.2
Secondary Building Units (SBUs): The Design Principles of MOFs

In contrast to molecular building blocks in general [7], which also include single metal nodes, SBUs are defined as an aggregate of metal ions stitched together by multidentate functional groups, such as carboxylates, into clusters (Figure 3.1) [1a].

The SBU term was coined for MOFs as an analogy to SBUs in zeolite chemistry, which are finite or infinite component units that facilitate the structural diversity

The Chemistry of Metal–Organic Frameworks: Synthesis, Characterization, and Applications, First Edition. Edited by Stefan Kaskel.

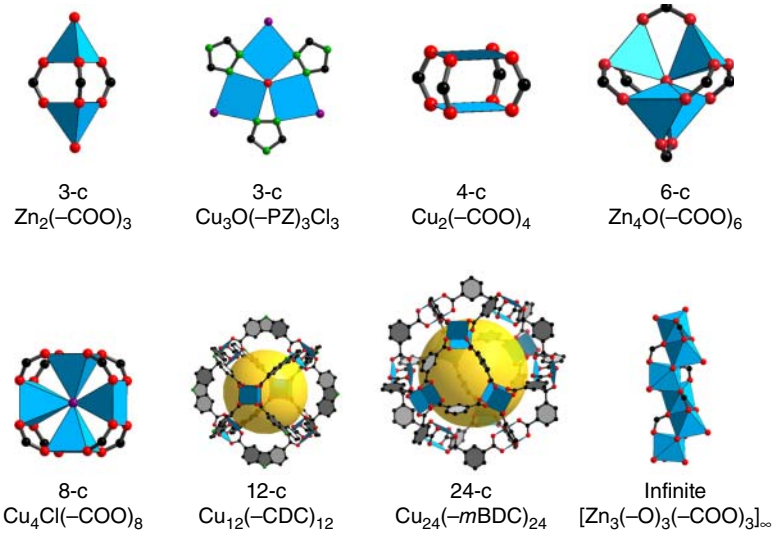

Figure 3.1 Selected M–O or M–N clusters that can serve as SBUs in MOFs and are made from zinc and copper; *n*-c describes the connectivity of the node. Color code: black, C; red, O; green, N; purple, Cl; and blue polyhedra, Zn, Cu (PZ, pyrazolate; AD, adeninate; CDC, 9*H*-carbazole-3,6-dicarboxylate; and *m*BDC, 1,3-benzenedicarboxylate). The yellow ball represents the free space in the building unit.

of zeolites. In MOFs, these SBUs serve as rigid vertices propagated into a framework by strong bonds with rigid organic struts, thus accounting for high structural stability. The decoration of these SBUs provides directionality, and they therefore serve as geometric prerequisites to the resulting MOF structure. Although MOFs have been significantly developed over the past decade resulting in over 20 000 structures known at present [8], there is still only a handful of high-symmetry SBUs that have sustained nets that can be described as "default" nets [9] obtained by direct, linear linking of polygons or polyhedra. These default nets are particularly useful, since they allow for more elaborate linker design such as functionalization or expansion, without altering the underlying net topology. For the description of net topologies presented throughout this chapter, we use abbreviations in the form of three-letter codes as provided by the Reticular Chemistry Structure Resource (RCSR) database [10]. If necessary and not given in the original contribution, we determined the topology using the program package TOPOS [11].

3.3 Points of Extension

Points of extension in MOF chemistry mean the number of possible connections between one metal cluster and other metal clusters through organic linkers [12].

In the case of MOF-5 [13], the $Zn_4O(–COO)_6$ cluster contains six carboxylate carbons (the points of extension) that serve as vertices of an octahedral-shaped building unit. In this chapter, we will classify the SBUs according to their points of extension from 3 to 12. Additionally, we outline SBUs derived from higher connected metal–organic polyhedra (MOPs) that can principally serve as 12- or 24-connected nodes if they are regarded as one entity without deconstruction [14]. Infinite, rod-like SBUs that are composed of one-dimensional cluster chains rather than discrete entities complete our contribution. Furthermore, the highlighted cluster geometries are exemplified by at least one structure that is considered prototypal for an isoreticular (of the same net topology) class of MOFs and demonstrated amenable to fine-tuning of structure/property relationships such as ultrahigh surface area. These prototypes are not necessarily the default nets; however they represent – from our viewpoint – the predominant frameworks for that particular cluster.

3.3.1
Three Points of Extension

Frameworks of 3-c nets are very common and have mostly $SrSi_2$ (**srs**) or $ThSi_2$ (**ths**) topologies [15]. They are mainly based on single metal nodes that are extended with pyridine- or nitrile-type linkers. A compound with formula $Cu(BIPY)_2(PF_6)$ composed of Cu^I and 4,4′-bipyridine (BIPY) was the first structure to be termed metal–organic framework, abbreviated to MOF in 1995 [16]. However, we seek to only emphasize higher nuclear clusters and therefore exclude any frameworks based on single metal nodes.

Besides 4-c paddle wheel SBUs that represent a very common structural motif in MOF chemistry, there are a few reports on $Zn_2(–COO)_3$ paddle wheels that serve as 3-c nodes. In 2006, it was reported that when $Zn(NO_3)_2$ is reacted with NH_2-H_2BDC (NH_2-H_2BDC = 2-amino-1,4-benzenedicarboxylic acid) in *N*,*N*-diethylformamide (DEF), in the presence of a cross-linked copolymer, PNMOF-3 $Zn_4(NH_2\text{-BDC})_3(NO_3)_2$ was isolated (Figure 3.2) [17]. This is in contrast to the results from conventional synthesis, where IRMOF-3, the amino-functionalized variant of MOF-5, is typically obtained [18]. The copolymer, consisting of methacrylic acid and divinylbenzene and used in various ratios, provided a different environment for MOF formation. PNMOF-3 crystallizes in a hexagonal space group with 3-c Zn-paddle wheels that contain one nitrate ion and one water molecule at the remaining tetrahedral coordination site. The eclipsed arrangement of the layers enables the formation of hexagonal channels which are 14.9 Å in diameter. This building unit was additionally reported in extended nets based on 1,3,5-benzenetricarboxylate (BTC) [19] and a rhombic dodecahedral MOP [20]. Moreover, it produces a tetrahedral building unit such as $[Zn_2(COO)_3(COO)]$, with the same core structure in the trinodal 3,3,4-c USF-4 [21].

Another common cluster motif is represented by the triangular azolate-based $Cu_3O(–PZ)_3X_3$ (X = Cl, OH), where each Cu is square planar coordinated by one

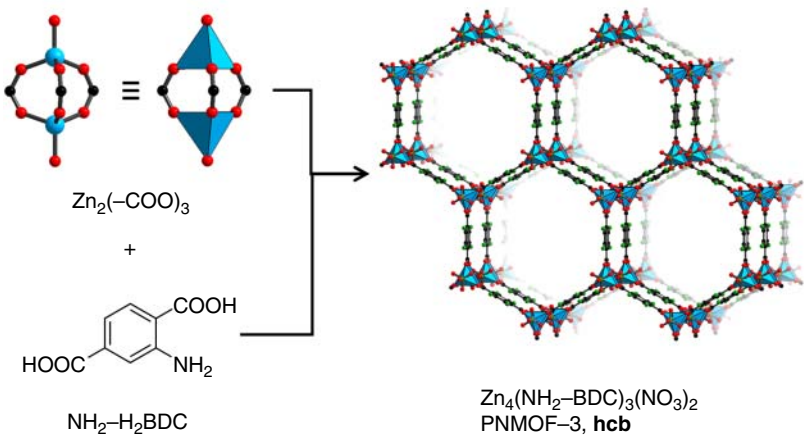

Figure 3.2 Single-crystal X-ray structure of PNMOF-3 along [001]. The hexagonal channels of 14.9 Å in diameter are clearly visible. Hydrogen atoms are omitted for clarity. NH_2 groups are disordered over four positions with occupancy 1/4. Color code: black, C; red, O; green, N; and blue polyhedra, Zn.

μ_3-oxygen, two bidentate pyrazole moieties, and a terminal anionic ligand such as chloride or hydroxide.

When these building blocks are joined with linear 4,4′-bi(1,2,4-triazole) (BTR) linkers, a 3-c **srs** topology net is obtained (Figure 3.3) [22]. Here, the nonplanar geometry of the linker accounts for the formation of an **srs** rather than an **hcb** net. This framework is eightfold interpenetrated, which leads to almost all of the void space being occupied. A closely related trimeric building unit also occurs in MOFs based on the 3,24-c rhombicuboctahedron triangle (**rht**) net [23], which will be discussed later.

3.3.2
Four Points of Extension

Copper and zinc (in the +II oxidation state) behave relatively similar with respect to cluster formation when combined with carboxylates in a ratio of 1 : 2 and typically afford the square paddle wheel.

The large library of MOFs having these SBUs relies primarily on elaboration of linker design and thus facilitates the generation of ultrahigh surface area materials. A specific class of building blocks, the MOPs [24] that are principally composed of paddle wheel entities, will be discussed later. The well-known paddle wheel cluster motif appears in the structures of molecular copper(II) acetate as well as chromium(II) and rhodium(II) acetates [25]. Each Cu^{2+} is five-coordinated in this case by four carboxylate oxygens, and the free coordination site is usually occupied by a water/solvent ligand.

In 1998, MOFs having robust metal–carboxylate clusters gained momentum, since microporosity by surface area and pore volume determination

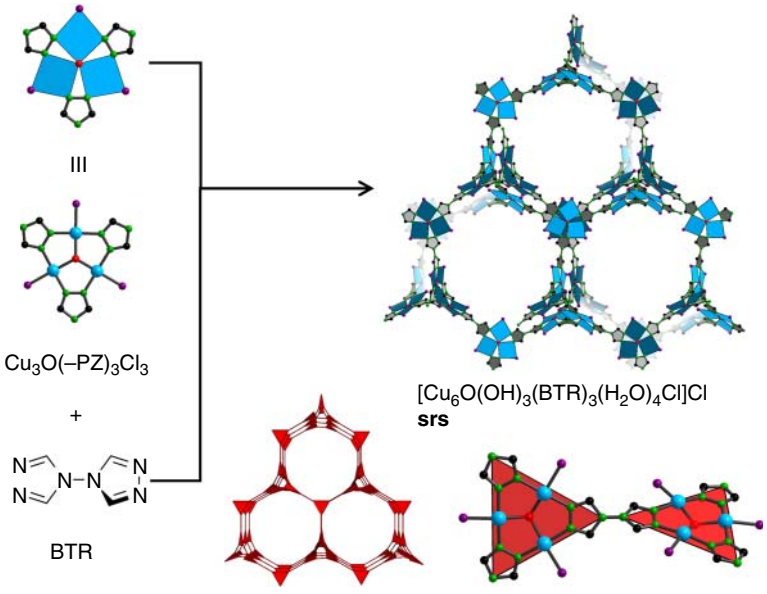

Figure 3.3 Combination of $Cu_3(OH)(–PZ)_3X_3$ (X = Cl, OH) and the linear BTR linker that generates an overall 3-c **srs** net. The structure and the underlying **srs** net (augmented version) are shown along [111]. Interpenetrating networks and hydrogen atoms are omitted for clarity. Color code: black, C; red, O; green, N; purple, Cl; and blue polyhedra, Cu.

was discovered [26]. A material termed MOF-2 with formula $Zn(BDC)(H_2O)$ (H_2BDC = benzene-1,4-dicarboxylic acid) was synthesized and shown to have voids filled with guest molecules, such as *N*,*N*-dimethylformamide (DMF) and H_2O, respectively (Figure 3.4). The structure is built from $Zn_2(–COO)_4(H_2O)_2$ paddle wheel building units that are further linked through BDC struts. The resulting two-periodic square-grid net (**sql**) gains additional stability through strong hydrogen bonding interactions between the layers and by the axial water molecules as well as the carboxylate moieties on the paddle wheel units.

The permanent porosity of MOF-2 was established from gas adsorption studies. First, guests were removed under vacuum with heating to yield the desolvated structure Zn(BDC). Experimental isotherms using nitrogen at 77 K then revealed a type I behavior and enabled the estimation of Langmuir surface areas between 270 and 310 $m^2\,g^{-1}$, as well as micropore volumes between 0.094 and 0.086 $cm^3\,g^{-1}$ (Figure 3.5).

3.3.3
The Discovery and Importance of Open Metal Sites

After the discovery of porosity in MOFs, the introduction of open metal sites (OMS) represents another major step forward to functional materials with

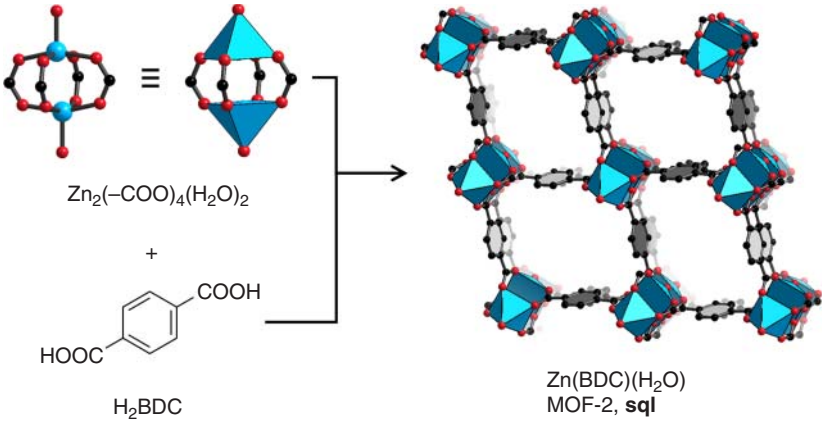

Figure 3.4 View of the desolvated MOF-2 structure along the crystallographic [001] direction; the rectangular channels are clearly visible. Hydrogen atoms and solvent molecules are omitted for clarity. Color code: black, C; red, O; and blue polyhedra, Zn.

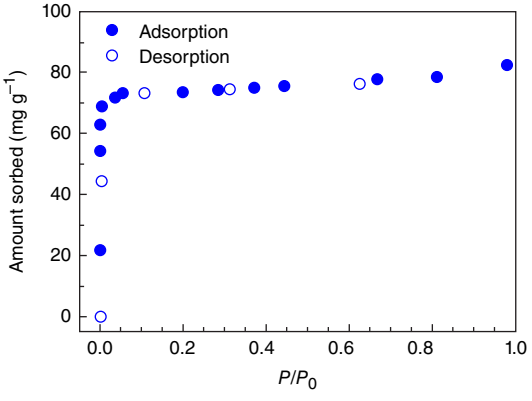

Figure 3.5 Gas adsorption isotherm for MOF-2 probed with nitrogen at 77 K. This served as the first example of microporosity reported in an MOF.

hitherto unexplored properties. In 2000, square Cu-paddle wheels were linked with tetrahedral ATC (H_4ATC = adamantane-1,3,5,7-tetracarboxylic acid) to afford MOF-11 with formula $Cu_2(ATC)\cdot 6H_2O$ [27]. This material exhibits the previously reported 4,4-c **pts** topology [27] based on square and tetrahedral building units (Figure 3.6).

Interestingly, the as-synthesized form of MOF-11 $Cu_2(ATC)\cdot 6H_2O$, where the Cu-paddle wheel OMS are occupied by water molecules, crystallizes in the monoclinic space group *C*2/*c*. After full evacuation and removal of all water molecules, the dehydrated form undergoes a change in symmetry to tetragonal *P*. The Langmuir area of this compound was estimated to be 560 $m^2\,g^{-1}$ and represents the first permanently porous architecture that revealed covalently held OMS.

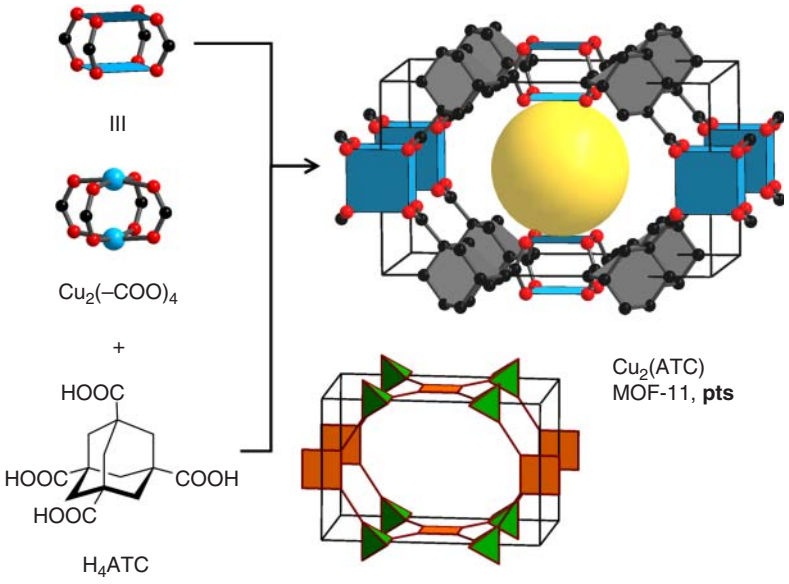

Figure 3.6 Single-crystal X-ray structure of the guest-free (tetragonal) form of MOF-11. The Cu-paddle wheels display open metal sites (OMSs) pointing into the interior of the pore. Augmented **pts** net, consisting of squares and tetrahedra in a ratio of 2 : 1 (right). Color code: black, C; red, O; and blue polyhedra, Cu. The yellow ball represents the empty space in the framework.

Another prototypal MOF termed HKUST-1 (HKUST = Hong Kong University of Science and Technology) is a well-known material sustained by Cu-paddle wheel building units [28]. $Cu_2(–COO)_4$ SBUs are linked to BTC entities (H_3BTC = benzene-1,3,5-tricarboxylic acid), resulting in an overall binodal 3,4-c twisted boracite (**tbo**) net with the formula $Cu_3(BTC)_2(H_2O)_3$ (Figure 3.7) [29].

The removal of the terminal water ligands is feasible and produces the anhydrous form $Cu_3(BTC)_2$, accompanied by a color change of the material from blue to purple. Surface area analysis was performed with nitrogen at 77 K and yielded a Brunauer–Emmett–Teller (BET) area of around 700 $m^2\,g^{-1}$, which indicates a not fully desolvated structure. More recent BET measurements of this material yielded around 1800 $m^2\,g^{-1}$ after full activation [30].

HKUST-1 is indeed a modular structure and can be expanded by means of reticular chemistry as exemplified by PCN-6′ [31] and MOF-399 [32], of which the latter currently holds the world record for the lowest-density MOF reported (0.126 $g\,cm^{-3}$). Recently, a series of MOFs was examined with respect to methane storage, and it was shown that materials such as UTSA-20 [33] or PCN-14 [34] were outperformed by HKUST-1 in terms of volumetric uptake. The authors therefore suggested that HKUST-1 to be used as the gold standard for the development of new methane storage materials [35].

We would like to note here that other isostructural variants of HKUST-1 also exist and are based on different metal paddle wheel SBUs [36]. In contrast to the

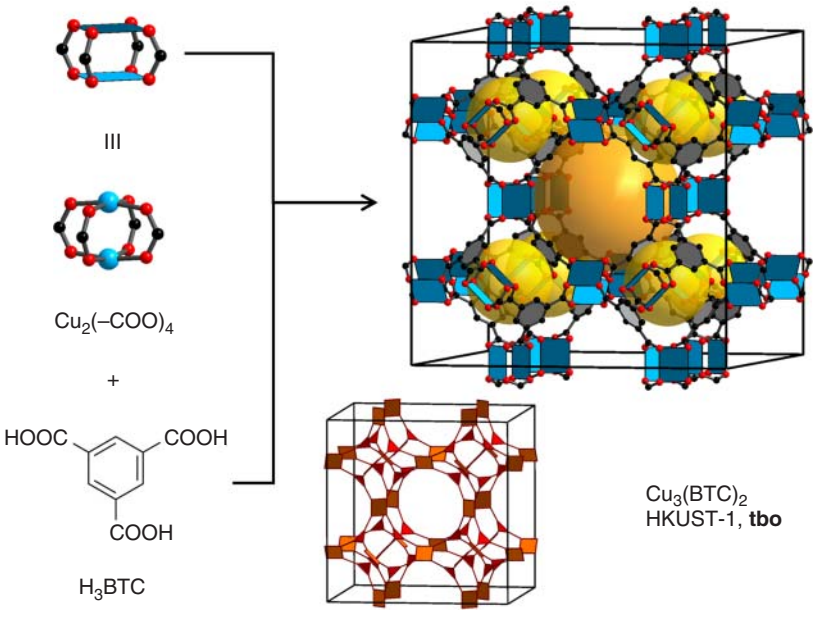

Figure 3.7 The combination of $Cu_2(–COO)_4$ and BTC affords HKUST-1. The underlying topology is a 3,4-c **tbo** net. Hydrogen atoms and solvent molecules are omitted for clarity. Color code: black, C; red, O; and blue, Cu. The yellow and orange balls represent the empty space in the framework.

Cu-paddle wheel, the zinc variant of HKUST-1 exhibits no microporosity as exemplified by its negligible uptake of N_2 at 77 K. It was demonstrated that by using positron annihilation spectroscopy, HKUST-1-Zn suffers from an inherent surface instability after solvent removal and therefore appears nonporous [36b]. This study, along with another [37], showed that the nature of the metal cation in the cluster might be essential to address material stability and thus practical utility.

After combining permanent porosity together with OMS, it was demonstrated that such structures could be ideal as hydrogen sorption materials [38]. A framework termed MOF-505 demonstrated that the combination of Cu-paddle wheel SBUs together with rectangular BPTC linkers (H_4BPTC = 3,3′,5,5′-biphenyltetracarboxylic acid) affords a 4,4-c **nbo**-type net (Figure 3.8). Topological deconstruction approaches recently suggested that this linker could be regarded as two linear connected triangular moieties (*m*BDC derivative, *m*BDC = 1,3-benzenedicarboxylate). This renders the overall uninodal, edge-transitive **nbo** net into a 3,4-c binodal, edge-two-transitive **fof** topology [14]. In detail, MOF-505 is principally built from undulating kagomé (**kgm**) 2D hexagonal layers [39] that are constructed from $Cu_2(–COO)_4$ paddle wheel SBUs and *m*BDC moieties. These layers are in turn connected through the 5-position of *m*BDC in a staggered conformation (Figure 3.8) [30]. We would like to point out that MOF-505 was not the first **nbo** net reported.

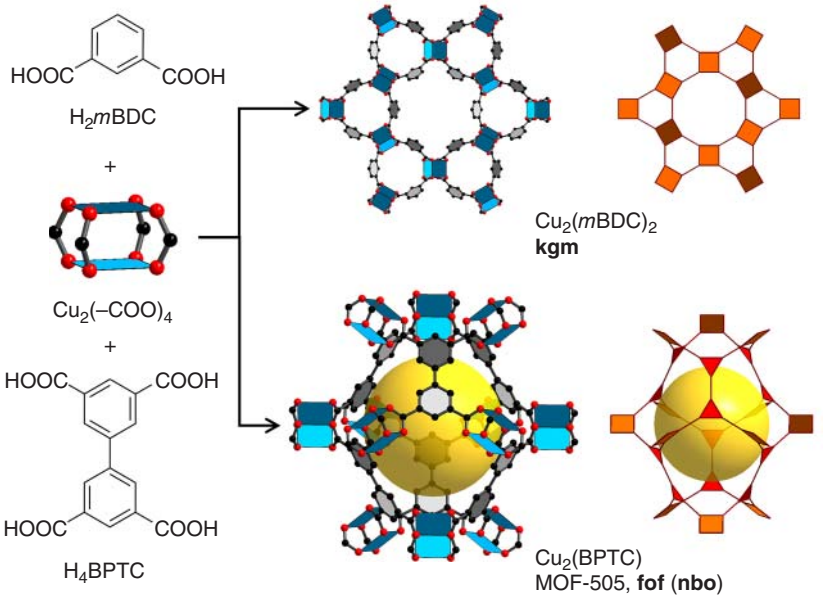

Figure 3.8 The **nbo**/**fof** net (MOF-505) sustained by a tetracarboxylate linker. The overall structure can be viewed as linker-to-linker cross-linked hexagonal kagomé (**kgm**) layers that are in turn built from $Cu_2(–COO)_4$ paddle-wheel SBUs and *m*BDC moieties. Hydrogen atoms are omitted for clarity. Color code: black, C; red, O; and blue, Cu. The yellow ball represents the empty space in the framework.

The **nbo** topology was deliberately designed and then synthesized in 2001 by using a 2-Br-BDC linker (MOF-101); however permanent porosity and the occurrence of OMS, also with respect to enhanced sorption properties, were not addressed at that time [40]. The fully activated MOF-505 displays a Langmuir surface area of 1830 $m^2\ g^{-1}$ and a high hydrogen uptake of 2.47 wt%. The authors suggest the formation of Cu-OMS as the main contribution to the exceptionally high H_2 uptake capacity. These **nbo**/**fof** nets have since been derivatized, and the introduction of various functionalized tetracarboxylate linkers led to materials that demonstrated superior performance with respect to hydrogen, carbon dioxide, and methane sorption as well as CO_2 fixation and catalysis [34, 37, 41].

3.3.4
Six Points of Extension

Metal clusters that provide six points of extension can be divided into octahedral and trigonal prismatic geometries. In 1998, the first MOF built from an SBU with six points of extension, termed MOF-3, was reported exhibiting potential OMS [42]. The reaction of zinc nitrate hexahydrate together with H_2BDC in DMF and methanol (MeOH) afforded the as-synthesized structure $Zn_3(BDC)_3{\cdot}6MeOH$. Single-crystal X-ray diffraction revealed that the framework is composed of a

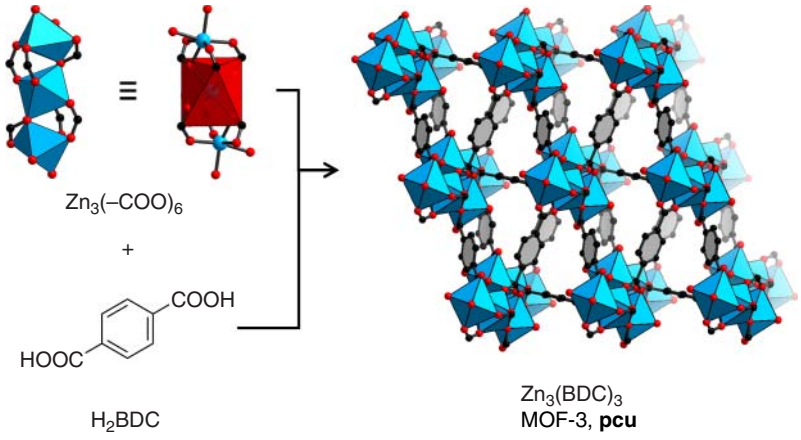

Figure 3.9 Single-crystal X-ray structure of MOF-3. Three octahedrally coordinated Zn^{2+} that are bridged by a total of six carboxylates form a distorted octahedral SBU (red) which also contains terminal MeOH ligands. Linking of these SBUs together by BDC affords MOF-3 with **pcu** topology. Color code: black, C; red, O; blue octahedra, Zn; and red octahedron, vertex figure.

$Zn_3(–COO)_6$ SBU, where each Zn^{2+} is octahedrally coordinated by six oxygen atoms, two of them being from MeOH ligands (Figure 3.9). The six points of extension (i.e., the –COO moieties) propagate in a distorted octahedral geometry and therefore generate a three-dimensional net with primitive cubic (**pcu**) topology. The presence of OMS was confirmed by introduction of various alcohols, ammonias, and primary/secondary amines into the pores of evacuated MOF-3. X-ray powder diffraction also confirmed the framework's integrity during liquid adsorption processes and after regeneration of the compound. Although the material is not permanently porous toward gases, it represented an important milestone with respect to selective inclusion of guest molecules and molecular recognition.

The prototype for octahedral clusters is represented by the well-known basic zinc acetate $Zn_4O(COOCH_3)_6$ [43]. It is composed of a tetrahedral central oxide surrounded by four tetrahedrally coordinated Zn^{2+} ions that are in turn bound by a total of six bridging carboxylate groups (COO^-). The carbon atoms of the carboxylate moieties serve as points of extension providing an octahedral decoration of the cluster (Figure 3.10). In 1999, these clusters were linked by linear BDC to obtain MOF-5 having the default **pcu** topology [13]. MOF-5 was synthesized through a solvothermal reaction of zinc nitrate tetrahydrate and H_2BDC in a mixture of DMF and chlorobenzene. The authors were able to show that the resulting framework contains voids filled with DMF and chlorobenzene guests, which are readily exchangeable with chloroform that could later be removed under vacuum at room temperature.

The desolvated crystals maintained their integrity, and nitrogen gas adsorption experiments at 77 K revealed a type I isotherm with an estimated Langmuir

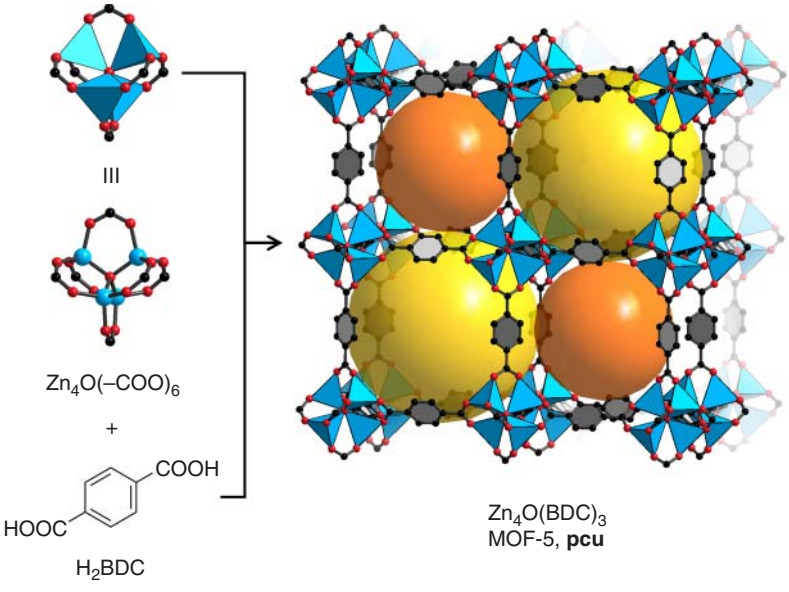

Figure 3.10 The three-dimensional structure of MOF-5. The two cavities are highlighted in yellow and orange, respectively. Color code: black, C; red, O; and blue tetrahedra, Zn.

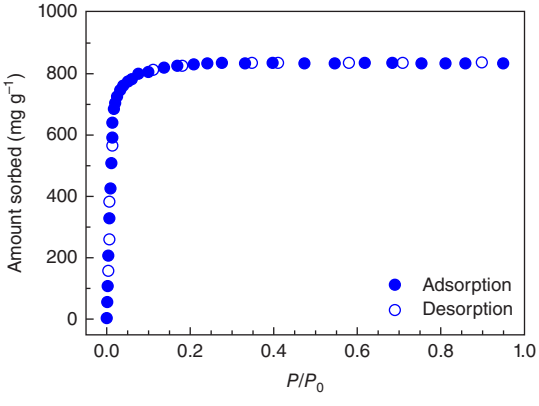

Figure 3.11 Gas adsorption isotherm of MOF-5 probed with nitrogen at 77 K. The graph clearly shows a type I isotherm, indicative of a microporous material.

surface area of 2900 $m^2\ g^{-1}$ and a pore volume of 1.04 $cm^3\ g^{-1}$ (Figure 3.11). At that time, these values far exceeded any known, conventional porous material such as zeolites, silicates, or porous carbon.

The enormous popularity of this structure, from our viewpoint, can be derived from three main reasons: It takes advantage of a simple network accessible through rational design principles, a facile route of preparation, and a very high porosity. It was later shown that MOF-5 is a modular structure, and several

isoreticular (**pcu** net) frameworks could be obtained by variation of length and functionality of the linker [18]. This enabled control over pore size and pore chemistry and led to materials with high methane storage capacity at room temperature and elevated pressure. However, the formation of twofold interpenetrated yet still isoreticular structures was observed based on linker size and synthetic conditions [44]. This phenomenon of interpenetration therefore drastically reduces the pore size of the MOFs, adversely affecting the generation of ultrahigh surface area materials. It was shown in other MOFs that this challenge could be addressed through variation of reaction temperature and concentration of starting materials [45].

Another strategy was applied in 2004, with the reporting of a highly porous framework, termed MOF-177 [46]. This structure was obtained by linking octahedral $Zn_4O(–COO)_6$ together with an expanded triangular linker (BTB = benzene-1,3,5-tribenzoate). The underlying 3,6-c net topology was identified as **qom** and recognized as superior over the possible rutile (**rtl**) and pyrite (**pyr**) nets, since **qom** does not show a self-duality and therefore interpenetration is inherently precluded. After activation, gas adsorption measurements revealed a Langmuir surface area of 4500 $m^2\,g^{-1}$ and a pore volume of 1.59 $cm^3\,g^{-1}$. This concept was followed up in 2010 by even further expansion of the triangular linker in order to obtain isoreticular **qom** nets (MOF-180, MOF-200) [47]. In such capacity, MOF-200 shows an exceptional Langmuir surface area of 10 400 $m^2\,g^{-1}$ and a BET area of 4530 $m^2\,g^{-1}$. In addition to isoreticular expansion, the use of mixed linkers – a linear and a triangular – enabled the synthesis of MOF-210 with **toz** topology. At the time of its synthesis, this material held the world record in BET area with a value of 6240 $m^2\,g^{-1}$ (Langmuir 10 400 $m^2\,g^{-1}$).

At present, $Zn_4O(–COO)_6$ SBUs are frequently utilized to produce high porosity nets [48], and the use of mixed linkers with this building block is especially feasible and has generated many heterogeneous MOF structures. In this context, especially multivariate MOFs that are based on the parent MOF-5 net and contain up to eight differently functionalized linkers showed superior performance when compared to their un- or monofunctionalized counterparts [49]. Very recently, this concept of heterogeneity within order has also proven fruitful with respect to the high surface area material MOF-177 [50].

Aside from pure carboxylate-based frameworks, it was demonstrated that the carboxylate moiety bound to the cluster could be partially replaced by pyrazolate (PZ)-type linkers in a way that retains the overall topology. The mixed $Zn_4O(BDC)(BPZ)_2$ MOF, in contrast to $Zn_4O(BDC)_3$, contains both bipyrazolate and terephthalate in a 2 : 1 ratio (Figure 3.12) [51]. We note here that the overall topology remains the same **pcu**; however the symmetry was reduced from cubic to tetragonal. This MOF shows a Langmuir surface area of 1900 $m^2\,g^{-1}$ together with a pore volume of 0.58 $cm^3\,g^{-1}$.

Reduction of symmetry from O_h to D_{3h} leads to trigonal prismatic clusters that are usually composed of a central oxide that is surrounded by three metal ions [52]. The octahedral coordinated metal ions are enclosed by four bridging carboxylates and a terminal ligand. The resulting cluster shows eclipsed carboxylates

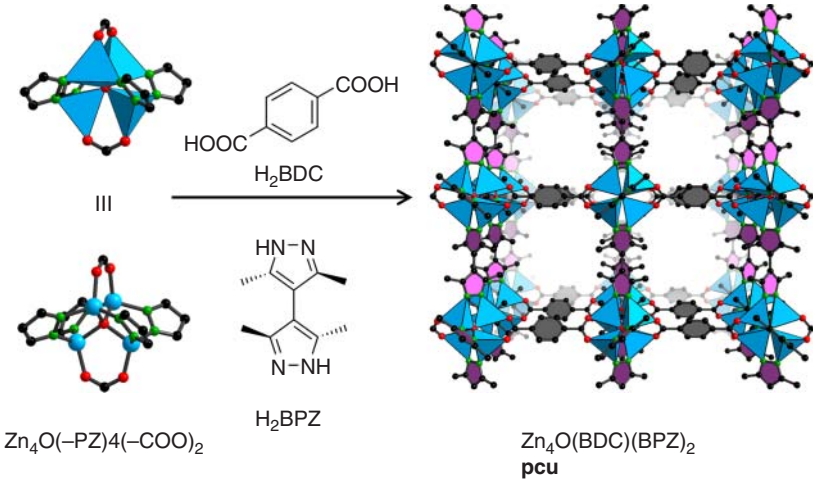

Figure 3.12 Partial replacement of the carboxylate moieties through pyrazole- (PZ) type linkers. The coordination complements the carboxylate motif in a 2 : 1 ratio. Mixed $Zn_4O(BDC)(BPZ)_2$ viewed along [100]; the underlying **pcu** net is clearly visible. Color code: black, C; red, O; and blue tetrahedra, Zn.

rather than staggered as observed in octahedral or trigonal antiprismatic geometries. Trigonal prismatic clusters of copper and zinc are reported in the literature, yet they remain uncommon with respect to other metal ions such as Cr^{3+} or Fe^{3+} that are very likely to form trigonal prismatic structures [53].

In 2010, a vertex-directed linker desymmetrization of networks was reported, based on the paddle wheel SBU [54]. The introduction of a nonsymmetric tricarboxylate linker, that is, the extension of one edge with respect to BTC, afforded a new framework termed UMCM-150 (Figure 3.13). This framework displays a high BET area of roughly 3000 $m^2\,g^{-1}$. Its underlying 3,4,6-c net topology (**agw**) consists of triangles, squares, and trigonal prisms. In this context, the trigonal prisms are geometric prerequisites to enable the sextuple cross-linking of hexagonal **kgm** layers built from Cu-paddle wheels and *m*BDC linkers. This building approach is similar to what was described as ligand-to-ligand cross-linking in the case of MOF-505 [38].

3.3.5
Eight Points of Extension

MOFs that are based on higher nuclearity SBUs are traditionally constructed from hard, highly charged metal cations such as Zr^{4+} [55] or Al^{3+} [56].

In 2006, a linker was designed based on three azolate moieties, 1,3,5-benzenetristetrazolate (BTT) that can serve as a 3-c node and links 8-c $Mn_4Cl(–PZ)_8$ SBUs into a hitherto unknown 3,8-c **the** topology net [57]. Later the isostructural variant with a $Cu_4Cl(–PZ)_8$ SBU was isolated as

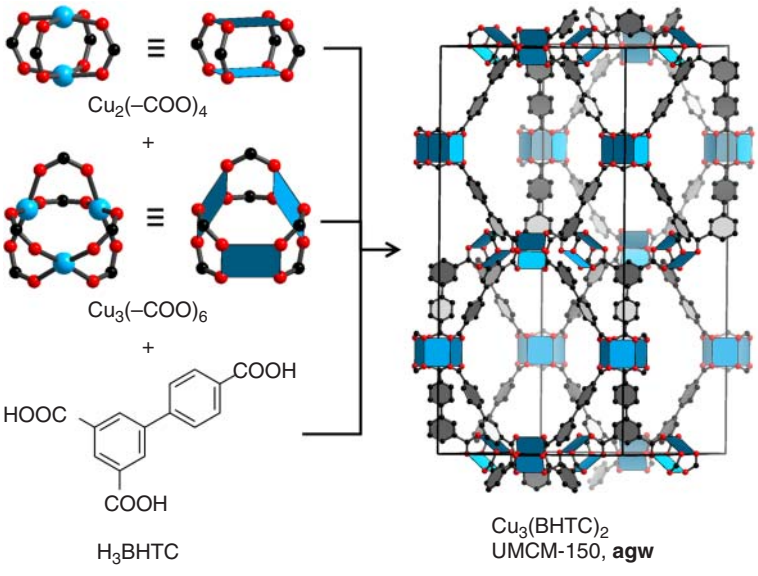

Figure 3.13 Single-crystal X-ray structure of UMCM-150. Cu-paddle wheel and trigonal prismatic clusters together with a desymmetrized tricarboxylate linker sustain the 3,4,6-c **agw** net. Alternating layers of undulating kagomé (**kgm**) and trigonal prisms are clearly visible. Color code: black, C; red, O; and blue polyhedra, Cu.

$H[Cu(DMF)_6][(Cu_4Cl)_3(BTT)_8(H_2O)_{12}]\cdot 3.5HCl\cdot 12H_2O\cdot 16CH_3OH$ (Figure 3.14) [58]. In contrast to the Mn variant (1100 $m^2\,g^{-1}$), the Cu framework could be fully desolvated and displays a BET area of 2100 $m^2\,g^{-1}$. The generated higher number of OMS also accounts for an overall higher hydrogen uptake at 77 K of 2.42 wt% at 77 K (2.25 wt% for Mn). The heat of adsorption was calculated to be around 6 kJ mol^{-1}.

A **the** topology framework based on a closely related $Cu_4Cl(-COO)_8$ SBU was reported in 2011 [59]. Similar to what has been done for MOF-5, where carboxylates could be substituted by PZ, the tetrazolates were shown to be fully replaced by carboxylates. This in turn means that the 8-c SBUs are connected through a shorter 3-c BTC linker. Figure 3.15 demonstrates that the underlying net topology can be simplified to an overall **sod** net; however, we believe that the description as a **the** net is more accurate. The authors reported that the pore partitioning effect of this anionic framework, which shows a BET area of around 800 $m^2\,g^{-1}$, led to an enhanced sorption capacity for carbon dioxide.

3.3.6
Nine Points of Extension

MOFs with nine points of extension built from Cu or Zn are very rare. To the best of our knowledge, it appears that there is only one example of a 9-c zinc cluster. This structure represented the first catalytically active MOF, and

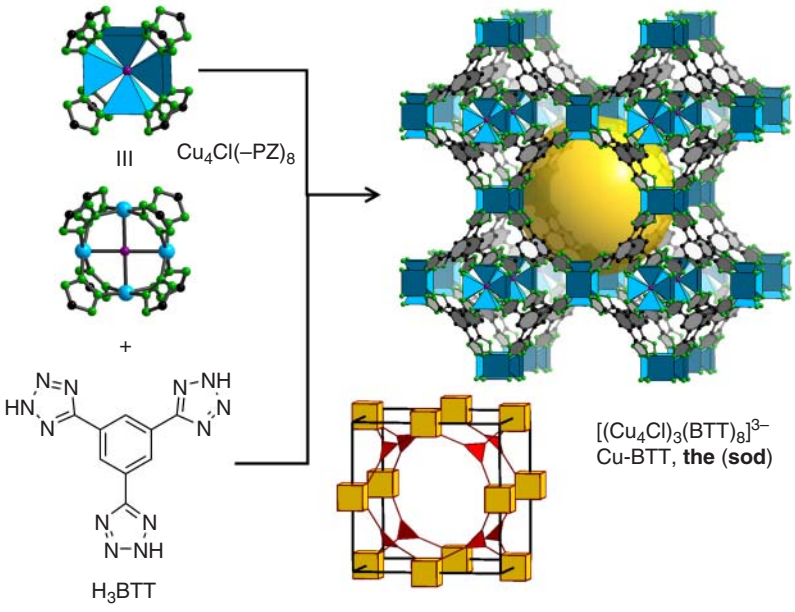

Figure 3.14 Single-crystal X-ray structure of the Cu-BTT-MOF along [100] (left). The underlying topology a 3,8-c **the** net is represented as the augmented version **the-a**. Color code: black, C; green, N; purple, Cl; and blue polyhedra, Cu. The yellow ball represents the open space in the framework.

it is constructed from zinc trigonal prisms together with a chiral D-tartaric or L-tartaric acid-derived linker (HD-DMPDC or HL-DMPDC = (4*S*,5*S*) or (4*R*,5*R*) 2,2-dimethyl-5-(pyridin-4-ylcarbamoyl)-1,3-dioxolane-4-carboxylic acid) to form homochiral frameworks named D-POST-1 or L-POST-1, respectively (Figure 3.16) [60]. Remarkably, the reaction of racemic 1-phenyl-2-propanol with either D-POST-1 or L-POST-1 enabled the formation of the corresponding esters with around 8% enantiomeric excess. The authors claimed that even though this %ee value is rather small, POST-1 represents the first ever reported asymmetric induction with respect to catalysis in an MOF.

3.3.7
Twelve Points of Extension

As in the case of MOFs with 8 points of extension, those with 12 points of extension made from copper or zinc are relatively rare. An unusual building unit, the $Zn_8(SiO_4)(–COO)_{12}$ SBU, is composed of a tetrahedral SiO_4 core that is in turn surrounded by tetrahedrally coordinated Zn^{2+} and decorated with 12 carboxylates around the exterior [61]. The 12 carboxylate linkers propagate in six directions and therefore provide double cross-linking with BDC to the nearest neighboring clusters, which renders the whole framework into a 6-c **pcu** net (Figure 3.17) [61b].

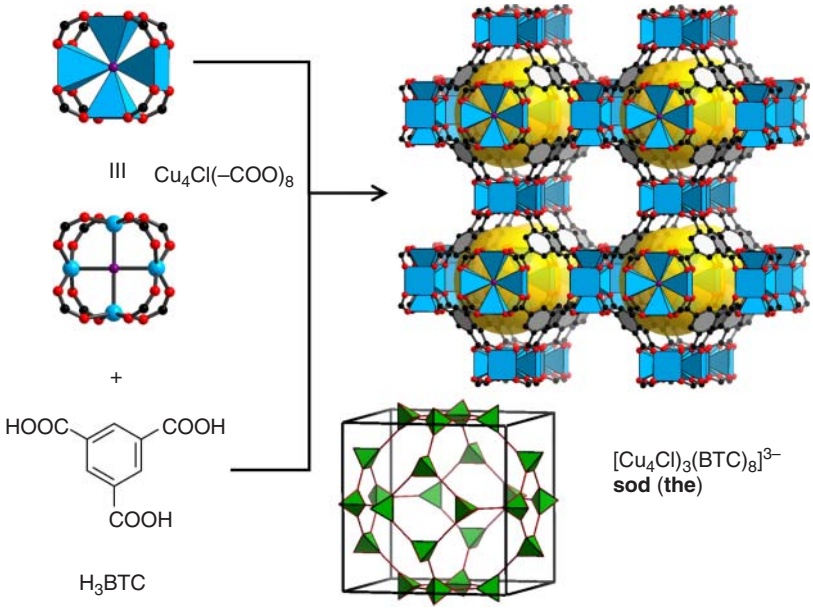

Figure 3.15 MOF built from $Cu_4Cl(–COO)_8$ SBUs that are in turn connected by BTC linkers. If each Cu^{2+} ion is considered as a tetrahedral node of the underlying topology, a **sod** net is obtained. Color code: black, C; green, N; purple, Cl; and blue polyhedra, Cu. The yellow ball represents the open space in the framework.

The open space in the structure is occupied by one identical interpenetrating net. This together with the double cross-linking is considered as the reason for both the high thermal stability of the compound up to 520 °C and its exceptional chemical stability. The authors also reported another framework based on the same cluster but using *m*BDC as a linker [61a].

In 2012, a highly porous MOF termed bio-MOF-100 was reported. This MOF is based on a 12-c zinc-adeninate building unit (ZABU) of formula $Zn_8O_2(AD)_4(–COO)_{12}$ (Figure 3.18) [62]. The ZABU contains 8 tetrahedrally coordinated Zn^{2+} and 4 adeninates (AD) as well as 12 exo-carboxylates that serve as points of extension. The geometry of the ZABU is a truncated tetrahedron (**tte**), where the tetrahedral vertex is triple cross-linked to a total of four neighboring clusters with linear BPDC (H_2BPDC = biphenyl-4,4′-dicarboxylic acid). Bio-MOF-100 therefore represents an overall 4-c net with **lcs** topology that differs from the common **dia** and the rare **lon** by the conformation of one of the six-membered rings (see Figure 3.19 for comparison). Bio-MOF-100 crystallizes in a cubic space group with cell parameters of 69.12 Å and a cell volume of 330 230 $Å^3$.

Furthermore, bio-MOF-100 represents the first reported MOF that contains only mesopores, and the large channels of 28 Å in diameter run along [110], [101], and [011]. The free volume of bio-MOF-100 was calculated to be around

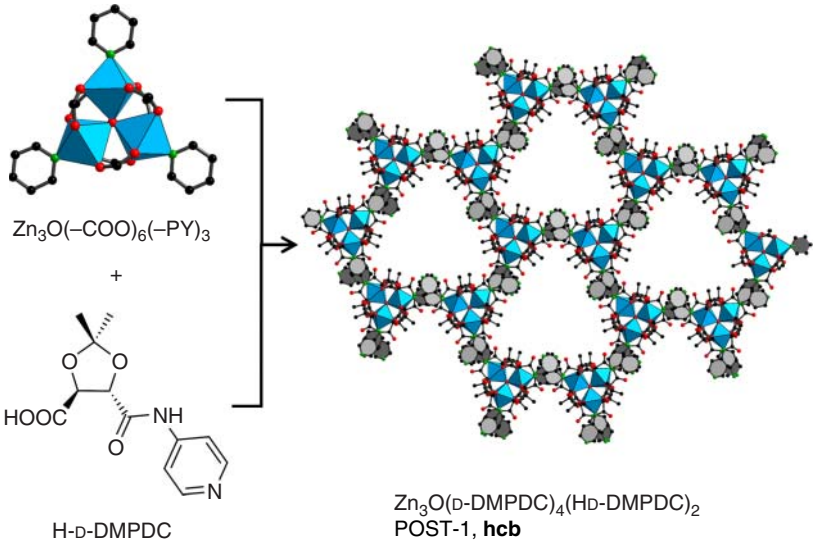

Figure 3.16 An unusual 9-c trinuclear $Zn_3O(–COO)_6(–PY)_3$ SBU, when reacted with the chiral linker D-HDMPDC, affords POST-1 that is composed of two-dimensional undulating hexagonal layers (**hcb**). The pores are running along [001] and provide space for catalytic, enantioselective transesterification reactions in their interior. Color code: black, C; green, N; and blue polyhedra, Zn.

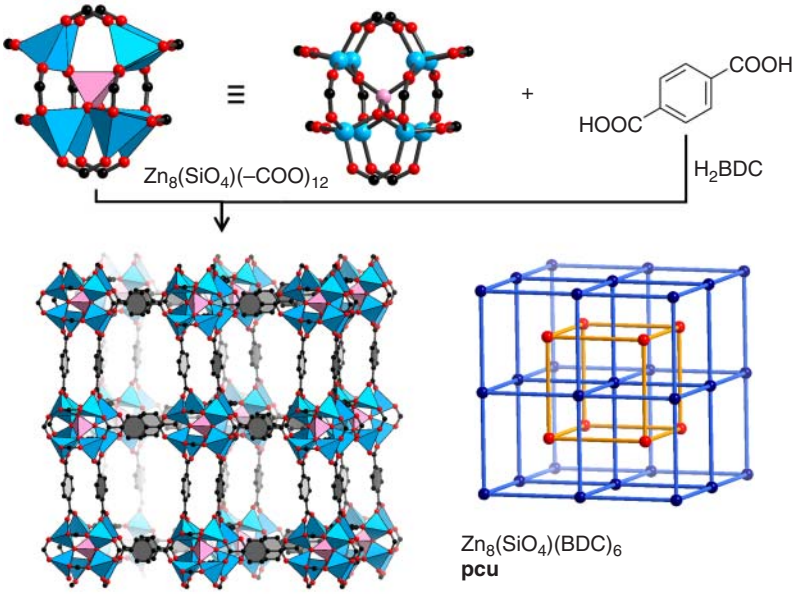

Figure 3.17 Double-walled **pcu** net built of $Zn_8(SiO_4)(–COO)_{12}$ SBUs together with BDC. The interpenetrating net and hydrogen atoms are omitted for clarity. Color code: black, C; red, O; blue tetrahedra, Zn; and pink tetrahedra, Si.

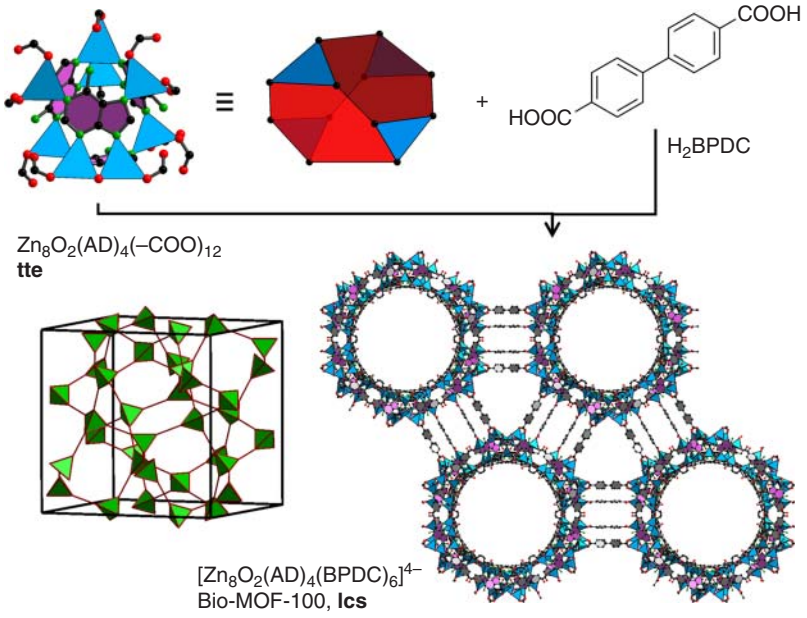

Figure 3.18 12-c $Zn_8O_2(AD)_4(–COO)_{12}$ ZABU that serves as an overall truncated tetrahedron. Each ZABU is triple cross-linked with BPDC to afford bio-MOF-100. Hydrogen atoms are omitted for clarity. Color code: black, C; red, O; green, N; and blue tetrahedra, Zn.

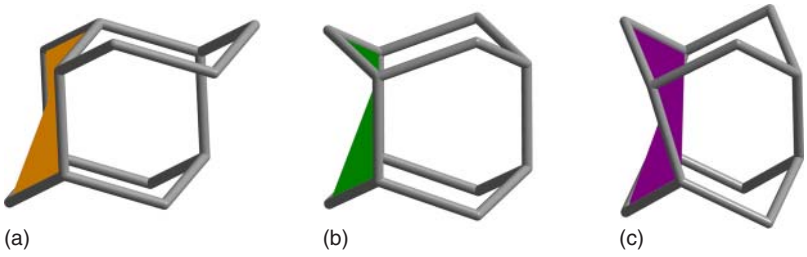

Figure 3.19 Difference between **dia**, **lon**, and **lcs** topology nets (from (a) to (c)). The chair conformation in **dia** and the boat conformation in **lon** are clearly visible. The **lcs** topology consists of a twist boat which rotates the six-membered rings along [001] by an angle of 60° with respect to each other.

85%, and after solvent exchange and activation with supercritical CO_2, a BET area of 4300 $m^2 g^{-1}$ and a pore volume of 4.3 $cm^3 g^{-1}$ were estimated from nitrogen gas adsorption isotherms at 77 K. It was later demonstrated that the carboxylate linkers in bio-MOF-100 are exchangeable by shorter or longer linkers and therefore provide the opportunity for postsynthetic linker exchange [63]. This enabled the fine-tuning of properties such as surface area and the formation of otherwise unattainable materials.

3.3.8
Twelve or Twenty-Four Points of Extension: Metal–Organic Polyhedra

In the previous sections we have discussed metal oxide-based clusters that can serve as SBUs in MOFs.

However, larger MOPs are also amenable to framework design and have demonstrated their ability to serve as high-connectivity building blocks, especially for the construction of highly porous materials [24]. Herein, the focus will be on structures derived from MOP-1 $Cu_{24}(m\text{BDC})_{24}$ [64] with **rco** topology that can act as a 12-c or 24-c building block (Figure 3.20).

MOP-1 was first reported in 2001 through the reaction of $Cu(NO_3)_2$ with H_2mBDC in a mixture of DMF and ethanol (EtOH). This discrete polyhedron is composed of 12 Cu-paddle wheel units that when connected with 24 *m*BDC linkers produce a truncated cuboctahedron (**cuo**) with an average cavity diameter of 15 Å (direct distance; without vdW radius) and a volume of 1766 $Å^3$. In the same year, this MOP was modified through the use of functionalized *m*BDC derivatives at its 5-position [65]. This resulted in a family of exteriorly decorated nanoballs that are principally based on the same polyhedron. In addition, a series of expanded as well as functionalized MOPs were reported [66]. These nanoballs potentially offer 12 points of extension on the OMSs of the outer Cu-paddle wheel moieties which renders them into cuboctahedral (**cuo**) building blocks. If they are linked through the 5-position of *m*BDC, a 24-c rhombicuboctahedral (**rco**) building block is obtained. 12-c polyhedra were practically achieved

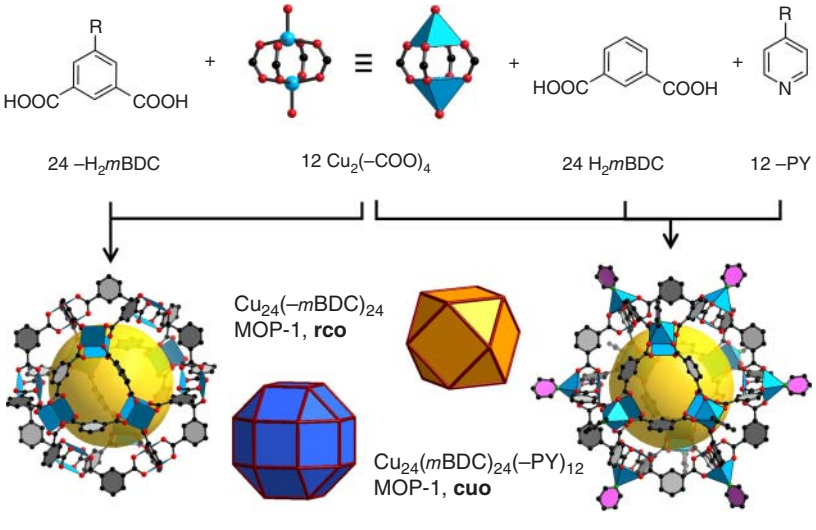

Figure 3.20 Construction of MOP-1 and its possibilities to serve as a 12-c **cuo**-node through functionalization of open metal sites or as a 24-c **rco**-node through extension of the *m*BDC-linker at its 5-position. Color code: black, C; red, O; green, N; and blue polyhedra, Cu. The yellow ball represents empty space in the building unit.

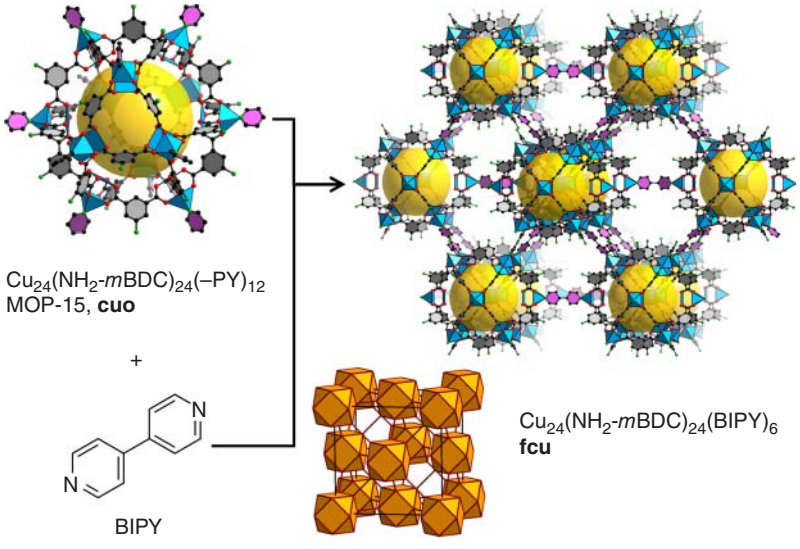

Figure 3.21 View of the 12-c polyhedral structure of the **fcu** net along [110]. Each MOP-15 is connected to 12 others via ditopic BIPY linkers. Color code: black, C; red, O; green, N; and blue polyhedra, Cu. The yellow ball represents empty space in the framework.

through replacement of the ligand at the OMS with a ditopic linker, such as BIPY (Figure 3.21).

First, the readily soluble MOP-15 $Cu_{24}(NH_2\text{-}m\text{BDC})_{24}$ [66a] was prepared and subsequently reacted with BIPY in *N*,*N*-dimethylacetamide (DMA) to afford an **fcu** net [67]. This MOF consists of three types of cages, the MOP, a tetrahedral, and a central mesoporous octahedral cage.

In 2007, it was first realized that these polyhedra could be linked due to their octahedral symmetry (O_h) into quadruple cross-linked **pcu** nets by using a flexible tetracarboxylate based on the *m*BDC motif [68]. The linker 1,3-bis(5-methoxy-1,3-benzene dicarboxylic acid)benzene (H_4BMBDB) provides this flexibility, and together with $Cu(NO_3)_2$ in a mixture of dimethyl sulfoxide (DMSO) and dichlorobenzene afforded the predicted MOF. In the three-dimensional framework, each polyhedron propagates into six directions, with four linkers to the nearest neighbor polyhedron (Figure 3.22).

The most popular topology based on MOP building units is the 3,24-c **rht**, which was realized in 2008 and has provided the foundation for extensive research [23]. This topology was theoretically predicted [69] as the only possible outcome to connect a triangular and an **rco** building unit that contains the same edge arrangement as a **cuo** into a network (Figure 3.23). Recent topological deconstruction approaches suggested that **rht** could also be represented as a 3,4,4-c **ntt** net [14]. The parent structure is based on two types of copper clusters and a bifunctional tritopic linker. This **rht**-MOF-1 was obtained by a one-pot self-assembly of 5-tetrazoylisophthalic acid (H_3TZI) together with $Cu(NO_3)_2$ in

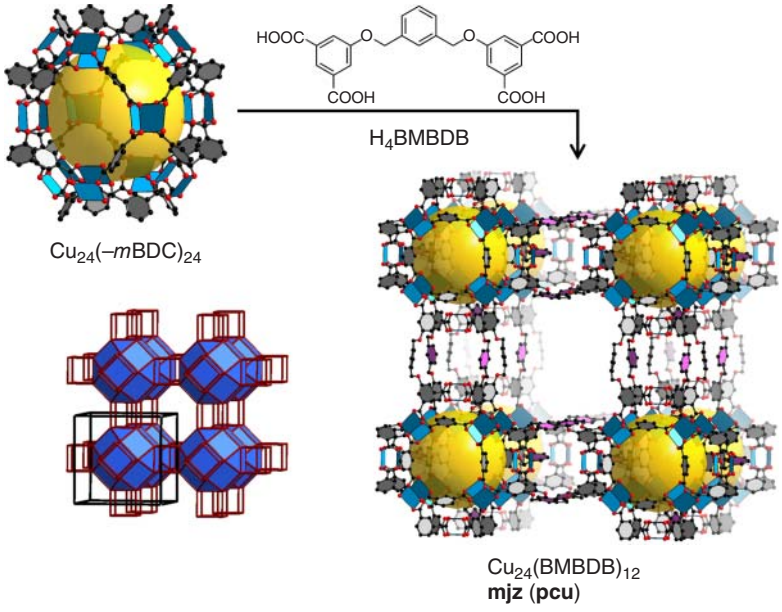

Figure 3.22 Quadruple cross-linking of metal–organic polyhedra into an **mjz** net that could be further simplified to an overall **pcu** net. Only one net of the twofold interpenetrated structure is shown, and hydrogen atoms are omitted for clarity. Color code: black, C; red, O; and blue, Cu. The yellow ball represents the empty space in the framework.

a DMF/EtOH solution. Single-crystal X-ray diffraction analysis revealed that the structure consists of a rhombicuboctahedron (**rco**) and a $Cu_3O(–PZ)_3$ moiety that serves as the triangular SBU (Figure 3.23). The latter renders the framework into a cationic net that is charge balanced by nitrate counterions. After evacuation of the large solvent accessible volume of ~75%, the material displays BET and Langmuir surface areas of 2847 and 3223 $m^2\ g^{-1}$, respectively. Hydrogen sorption measurements also revealed an uptake of 2.4 wt% at 77 K and 1 atm together with a high isosteric heat of adsorption of 9.6 kJ mol^{-1}.

Over the past years many other research groups have spent significant efforts to explore variations of this particular net [70]. It was shown that based on length or functionality of the linker, different material properties could be targeted. These will not be particularly emphasized in this chapter, but we rather give an overview on the modularity of the structure and how the building blocks facilitate the formation of the net.

The original **rht**-MOF-1 could be expanded by means of reticular chemistry in two ways: (i) the augmentation of MOP-1 by introduction of a longer but branched (120°) moiety or (ii) the augmentation of the triangular linker by simple elongation (i.e., introduction of phenylene or acetylene units) (Figure 3.24).

Polyhedron expansion was demonstrated using 5′-(1*H*-tetrazol-5-yl)-1,1′:3′,1″-terphenyl-4,4″-dicarboxylic acid (H_3TZTDC) linker in place of H_3TZI [71]. This,

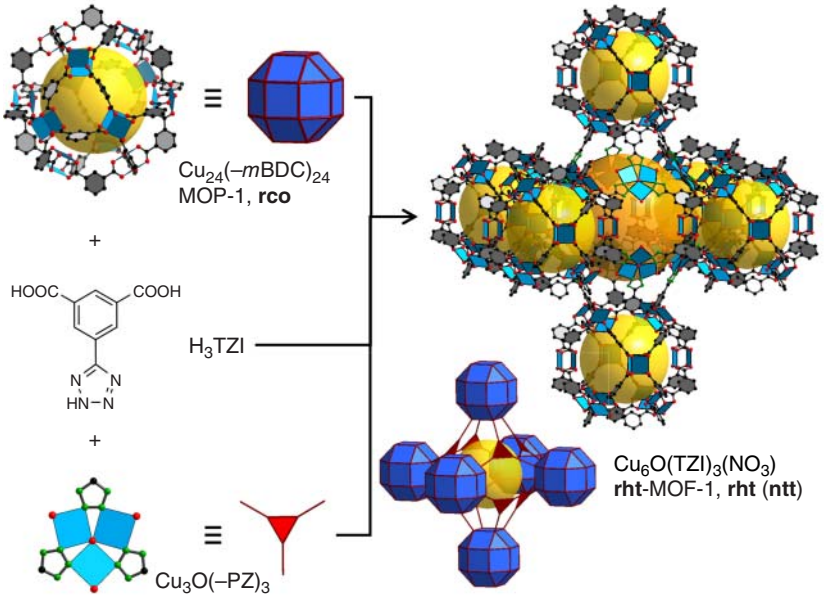

Figure 3.23 Schematic of **rht**-MOF-1 sustained by a Cu_{24}(–*m*BDC)$_{24}$ (**rco**) building block together with a triangular Cu_3O(–PZ)$_3$. The underlying topology (**rht**) is the only 3,24-c net possible as predicted. Hydrogen atoms are omitted for clarity. Color code: black, C; red, O; green, N; and blue polyhedra, Cu. The yellow and orange balls represent empty space in the framework.

in turn, generates an inner cavity diameter of 25.7 Å, which almost doubles that of **rht**-MOF-1. It was also previously demonstrated that the Cu_3O(–PZ)$_3$ building block can be replaced by a purely organic linker, a hexatopic carboxylate that is principally sustained by three isophthalate moieties. Whereas the *m*BDC entities spawn the polyhedral cage, their distance to the threefold branch can be varied in order to increase the spacing between the MOPs. Since this strategy was followed by many groups in the past, we would like to highlight one particular example, utilizing a long hexatopic linker (Figure 3.24, left) with an edge length of around 20 Å [72]. Reaction of this linker together with $Cu(NO_3)_2$ afforded NU-110 with the expected **rht** topology. After activation of the framework by supercritical CO_2 drying, sorption measurements (N_2, 77 K) revealed a BET area of 7140 $m^2\ g^{-1}$ and a pore volume of 4.40 $cm^3\ g^{-1}$. Both of these values represent the current records for any material known to date.

Another type of MOP that could further be linked into MOFs is based on 9*H*-carbazole-3,6-dicarboxylate (CDC) and provides 12 points of extension in a **cuo** geometry (Figure 3.25, left). In 2009, the discrete $Cu_{12}(CDC)_{12}$ was isolated from $Cu(NO_3)_2$ and H_2CDC in a mixture of DMA and EtOH [73]. This **cuo**-MOP consists of twelve CDC that exhibit an overall 90° angle between the carboxylate moieties that link a total of six Cu_2(–COO)$_4$ paddle wheel SBUs together. The resulting polyhedron shows an inner diameter of 12 Å. This building block was

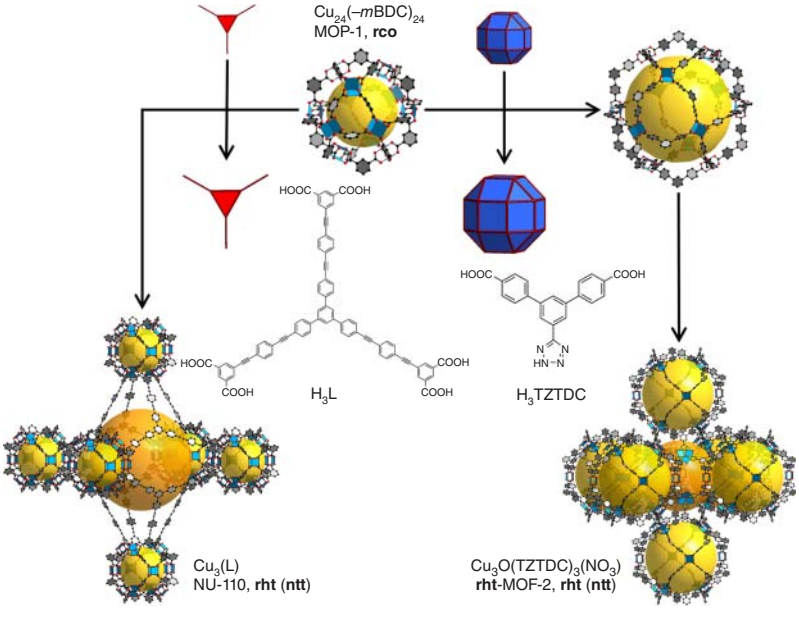

Figure 3.24 Modularity of the **rht** net: The original MOP-1 is isoreticular expanded leading to the recently reported **rht**-MOF-2 (bottom, right). Isoreticular expansion of the triangular linker (here using a phenyl moiety) results in the highly porous NU-110. Color code: black, C; red, O; green, N; and blue polyhedra, Cu. The yellow and orange balls represent empty space in the framework.

later linked with the tetratopic linker H_4BBCDC to afford a framework termed DUT-49 that displays an overall 12-c **fcu** topology [74]. Nitrogen gas adsorption isotherms at 77 K revealed a considerably high BET area of 5476 $m^2\ g^{-1}$. Moreover, due to its nearly optimal pore size, DUT-49 shows one of the highest methane uptake values (excess: 2.01 $g\ g^{-1}$; total: 2.45 $g\ g^{-1}$) at 50 bar in comparison with all other reported MOFs. Very recently, the authors synthesized a related linker (H_3CPCDC), which when combined with $Cu(NO_3)_2$ afforded DUT-75, an overall 4,12-c **ftw** net (Figure 3.25) [75]. In this case the **cuo** is considered as one building block that is linked together through a second $Cu_2(-COO)_4$ paddle wheel SBU. Therefore, the net could also be deconstructed to a 3,4,4-c net. DUT-75 and its isoreticular expanded variant DUT-76 display very high BET areas of 4081 and 6344 $m^2\ g^{-1}$, respectively, and demonstrate exceptional performance with respect to storage of methane and ethylene.

3.3.9
Infinite Secondary Building Units

MOFs based on discrete building units that are joined by organic linkers usually propagate into two or three dimensions. Aside from these, there are a handful of rod-like SBUs that are infinite in one dimension and are linked to each other via

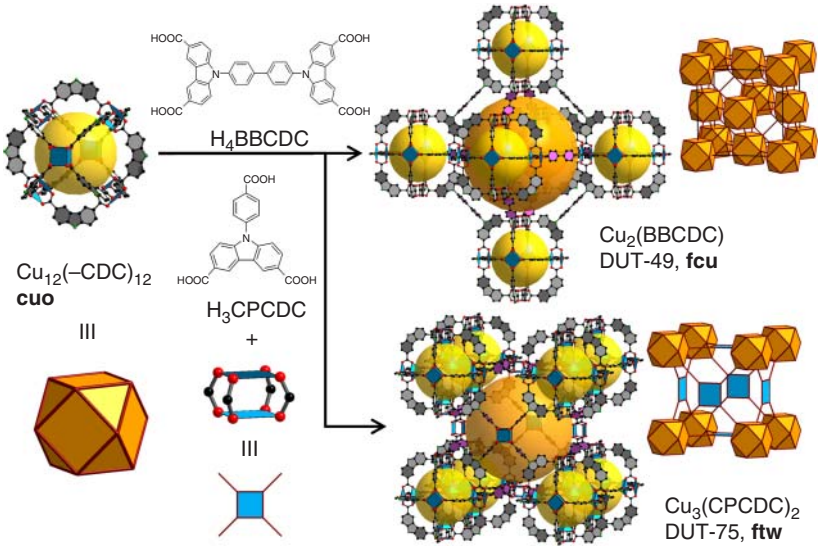

Figure 3.25 Schematic of linking a discrete **cuo**-MOP $Cu_{12}(–CDC)_{12}$ with linear linkers (DUT-49) or square nodes (DUT-75). High surface area materials with either **fcu** or **ftw** topology were afforded. Color code: black, C; red, O; green, N; and blue polyhedra, Cu. The yellow and orange balls represent empty space in the framework.

organic struts. One of the most prominent examples in this context is MOF-74 [76], a platform which represents the foundation of numerous studies including isoreticular expansion [77], integration of biomolecules, sorption of carbon dioxide [78] and hydrogen [79], and separation of various hydrocarbons [80], among others.

The parent MOF-74 structure $Zn_2(DOT)(DMF)_2{\cdot}2H_2O$ ($H_4DOT = 2,5$-dihydroxy-1,4-benzenedicarboxylic acid) was discovered in 2005. This structure is composed of infinite $[Zn_3(–O)_3(–COO)_3]_\infty$ rod-like SBUs that run along [001] and are linked into a hexagonal, three-dimensional network through DOT (Figure 3.26). The structure generates a **bnn** or **etb** net, depending on whether the hydroxo-functionalities are also considered as points of extension or if only the carboxylates are taken into account. The as-synthesized version of the MOF contains one molecule of DMF per zinc that is removable under vacuum and heating to make the 10.3 Å × 5.5 Å channels accessible.

Another important class of MOFs based on infinite SBUs is called bio-MOFs, and the most notable among them is bio-MOF-1 [81]. In 2009, a framework was reported that consists of infinite $[Zn_8O(AD)_4(–COO)_{12}]_\infty$ SBUs that when linked with BPDC affords the anionic bio-MOF-1 $(Me_2NH_2)_2[Zn_8O(AD)_4(BPDC)_6]$ that shows an overall **pcu** topology (Figure 3.27). The SBU, which could also be regarded as a discrete, double cross-linked 6-c $Zn_8O(–AD)_4(–COO)_{12}$, is composed of apex-sharing Zn-AD octahedral clusters that run along [001]. Gas adsorption experiments with nitrogen at 77 K revealed a microporous material with an estimated BET area of around 1700 $m^2\,g^{-1}$.

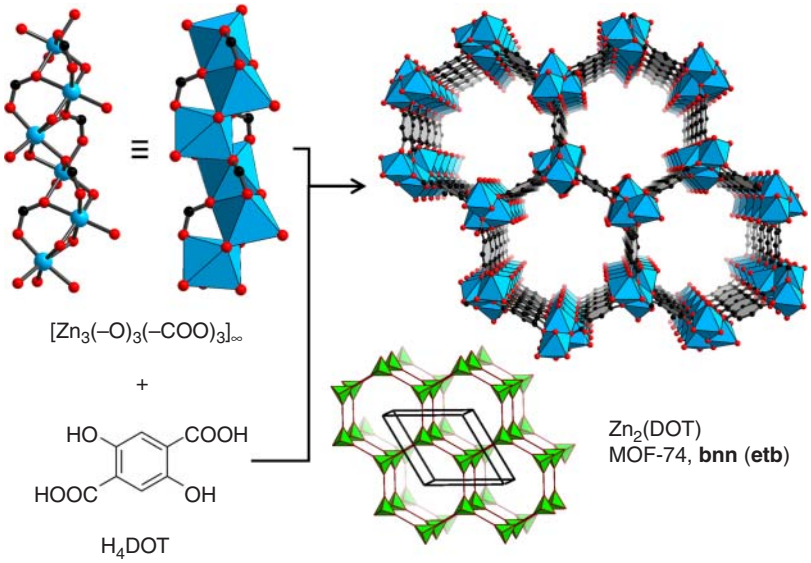

Figure 3.26 Parent MOF-74 $Zn_2(DOT)(DMF)_2 \cdot 2H_2O$ viewed along [001]. The hexagonal channels are clearly visible. Rodlike building units of formula $[Zn_2(–O)_2(–COO)_2]_\infty$ that are linked together by DOT spawn a **bnn** (shown here) or **etb** net, respectively. Color code: black, C; red, O; and blue polyhedra, Zn.

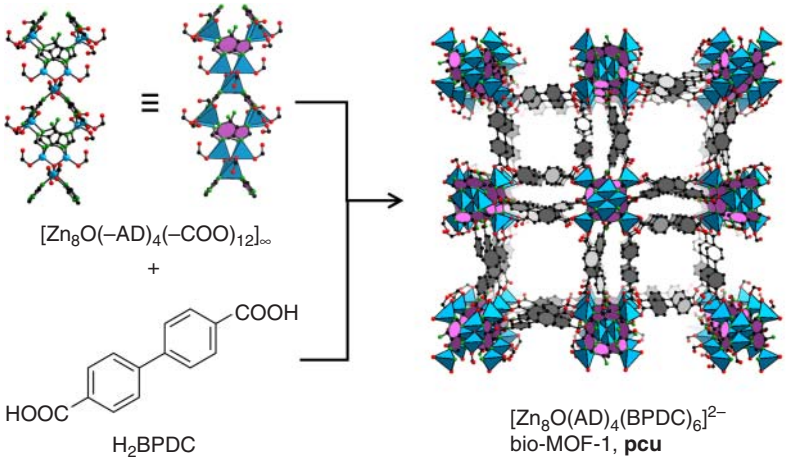

Figure 3.27 Infinite secondary building unit $[Zn_8O(AD)_4(–COO)_{12}]_\infty$ that sustains bio-MOF-1 (viewed along [001]). Color code: black, C; red, O; green, N; and blue polyhedra, Zn.

Since the framework of bio-MOF-1 is anionic, it was tested for its controlled drug release properties using procainamide HCl. After initial loading, this compound could then be released in a controlled manner by soaking the crystals in an aqueous buffer solution over the course of 20 h. It was thus demonstrated that anionic MOFs could be good candidates with respect to controlled drug release

Table 3.1 Summary of SBUs and related MOFs that are discussed in this chapter.

Points of extension[a)]	SBU	Compound name	Topology[b)]	REFCODE[c)]	References
3	$Cu(-PY)_3$		**ths**	ZIBRAD	[16]
	$Zn_2(-COO)_3$	PNMOF-3	**hcb**	ICITOE	[17]
	$Cu_3O(-PZ)_3Cl_3$		**srs**	WELTIR	[22]
	$Zn_2(-COO)_3$	MOAAF	**3,3,4,5-c**	PEJNUP	[19]
4	$Zn_2(-COO)_4$	MOF-2	**sql**	GECXUH	[26]
	$Cu_2(-COO)_4$	HKUST-1	**tbo**	FIQCEN	[28]
	$Cu_2(-COO)_4$	PCN-6′	**tbo**	NIBHOW	[31]
	$Cu_2(-COO)_4$	MOF-399	**tbo**	BAZGAM	[32]
	$Cu_2(-COO)_4$	MOF-11	**pts**	BIMDIL	[27]
	$Cu_2(-COO)_4$	MOF-101	**nbo**	YIXBIQ	[40]
	$Cu_2(-COO)_4$	MOF-505	**nbo, fof**	LASYOU	[38]
	$Cu_2(-COO)_4$	Kagomé	**kgm**	PACFOP	[39]
	$Zn_2(-COO_2)_3(-COO)$	USF-4	**3,4,4-c**	NAQLAT	[21]
	$Cu_2(-COO)_4$	MOP-1	**cuo, rco**	MIQCEU	[64]
	$Cu_2(-COO)_4$	MOP-15	**cuo, rco**	KOJXAJ	[66a]
	$Cu_2(-COO)_4$	**cuo**-MOP	**cuo**	SUPPID	[73]
6	$Zn_4O(-COO)_6$	MOF-5	**pcu**	SAHYIK	[13]
	$Zn_4O(-COO)_6$	MOF-177	**qom**	ERIRIG	[46]
	$Zn_4O(-COO)_6$	MOF-180	**qom**	CUSXIY	[47]
	$Zn_4O(-COO)_6$	MOF-200	**qom**	CUSXOE	[47]
	$Zn_4O(-COO)_6$	MOF-210	**toz**	CUSYAR	[47]
	$Zn_3(-COO)_6$	MOF-3	**pcu**	PURSOK	[42]
	$Zn_4O(-PZ)_4(-COO)_2$		**pcu**	WIYFAM	[51]
	$Cu_3(-COO)_6$	UMCM-150	**agw**	UKIQOV	[54]
8	$Cu_4Cl(-PZ)_8$	Cu-BTT	**the, sod**	VEXYON	[58]
	$Cu_4Cl(-COO)_8$		**the, sod**	ABEMIF	[59]
9	$[Zn_3O(-COO)_6(-PY)_3]$	POST-1	**hcb**	UHOPUC	[60]
12	$Zn_8(SiO_4)(-COO)_{12}$		**pcu**	OGIYEI	[61b]
	$Cu_{24}(m\text{BDC})_{24}(-PY)_{12}$		**fcu**	IVEKEA	[67]
	$Zn_8O_2(AD)_4(-COO)_{12}$	Bio-MOF-100	**lcs**	SAPBIW	[62]
	$Cu_{12}(-CDC)_{12}$	DUT-49	**fcu**	ACOCOM	[74]
	$Cu_{12}(-CDC)_{12}$	DUT-75	**ftw**	see SI	[75]
	$Cu_{12}(-CDC)_{12}$	DUT-76	**ftw**	see SI	[75]
24	$Cu_{24}(-m\text{BDC})_{24}$		**mjz, pcu**	CILLAL	[68]
	$Cu_{24}(-m\text{BDC})_{24}$	**rht**-MOF-1	**rht, ntt**	LIZWEX	[23]
	$Cu_{24}(-m\text{BDC})_{24}$	**rht**-MOF-2	**rht, ntt**	ADASAB	[71]
	$Cu_{24}(-m\text{BDC})_{24}$	NU-110	**rht, ntt**	SEMNIJ	[72]
∞	$[Zn_3(-O)_3(-COO)_3]_\infty$	MOF-74	**bnn, etb**	FIJDOS	[76]
	$[Zn_8O(AD)_4(-COO)_{12}]_\infty$	Bio-MOF-1	**pcu**	NUDLAA	[81]

a) Exodentate points where the framework could propagate into multiple dimensions.
b) Three-letter code as retrieved from the Reticular Chemistry Structure Resource (RCSR), if assigned. Two given codes for one compound arise from either deconstruction or simplification.
c) Unique six-letter code as retrieved from the Cambridge Structural Database (CSD), if assigned; otherwise see supporting information of the particular publication.

in vitro. Later the anionic nature of the framework was utilized for the exchange of organic cations which enabled the fine-tuning of CO_2 sorption properties [82].

3.4 Concluding Remarks

In summary, we have clearly shown that copper and zinc are amenable to the formation of many cluster entities due to their linkage through strong bonds with organic struts. We introduced the concept of SBUs and how they facilitate the formation of high-symmetry networks by means of reticular chemistry (Table 3.1). It was demonstrated that MOFs are special among all classes of materials since they allow for the rational design of clusters and thus predictable topological outcomes. This contrasts with MOFs sustained by phosphonates or sulfonates, which were therefore not further discussed. We also highlighted the properties of several of the materials presented, even if only very briefly, which emphasizes the importance of robust frameworks that preserve structural integrity and crystallinity. Therefore, it is highly anticipated that the reticular chemistry approach, based on SBUs, will play an important role for future custom designing of MOFs that are amenable for targeting specific applications.

Acknowledgment

Funding of MOF research in the Yaghi group is supported by BASF SE (Ludwigshafen, Germany). A. S. gratefully acknowledges financial assistance from the Deutsche Forschungsgemeinschaft (DFG, SCHO1639/1-1). The authors would like to thank Dr H. Furukawa and K. Cordova for the helpful discussions.

References

1. (a) Eddaoudi, M., Moler, D.B., Li, H., Chen, B., Reineke, T.M., O'Keeffe, M., and Yaghi, O.M. (2001) *Acc. Chem. Res.*, **34**, 319–330; (b) Moulton, B. and Zaworotko, M.J. (2001) *Chem. Rev.*, **101**, 1629–1658; (c) Kitagawa, S., Kitaura, R., and Noro, S.-I. (2004) *Angew. Chem. Int. Ed.*, **43**, 2334–2375; (d) Janiak, C. (2003) *Dalton Trans.*, 2781–2804.
2. Baerlocher, C., McCusker, L.B., and Olson, D.H. (2007) *Atlas of Zeolite Framework Types*, 6th rev. edn, Elsevier Science, Amsterdam.
3. Zhao, D., Feng, J., Huo, Q., Melosh, N., Fredrickson, G.H., Chmelka, B.F., and Stucky, G.D. (1998) *Science*, **279**, 548–552.
4. Zakhidov, A.A., Baughman, R.H., Iqbal, Z., Cui, C., Khayrullin, I., Dantas, S.O., Marti, J., and Ralchenko, V.G. (1998) *Science*, **282**, 897–901.
5. (a) Wells, A. (1954) *Acta Crystallogr.*, **7**, 535–544; (b) Wells, A. (1954) *Acta Crystallogr.*, **7**, 545–554.
6. Ockwig, N.W., Delgado-Friedrichs, O., O'Keeffe, M., and Yaghi, O.M. (2005) *Acc. Chem. Res.*, **38**, 176–182.
7. (a) Kaszynski, P., Friedli, A.C., and Michl, J. (1992) *J. Am. Chem. Soc.*, **114**, 601–620; (b) Gardner, G.B.,

Venkataraman, D., Moore, J.S., and Lee, S. (1995) *Nature*, **374**, 792–795.
8. Furukawa, H., Cordova, K.E., O'Keeffe, M., and Yaghi, O.M. (2013) *Science*, **341**, 1230444.
9. Sudik, A.C., Côté, A.P., and Yaghi, O.M. (2005) *Inorg. Chem.*, **44**, 2998–3000.
10. (a) O'Keeffe, M., Peskov, M.A., Ramsden, S.J., and Yaghi, O.M. (2008) *Acc. Chem. Res.*, **41**, 1782–1789; (b)RCSR http://rcsr.net (accessed 1 February 2016).
11. a Blatov, V.A. (2006) *IUCrCompComm Newsl.*, **7**, 4–38; (b)ToposPro http://topospro.com (accessed 1 February 2016).
12. Tranchemontagne, D.J., Mendoza-Cortés, J.L., O'Keeffe, M., and Yaghi, O.M. (2009) *Chem. Soc. Rev.*, **38**, 1257.
13. Li, H., Eddaoudi, M., O'Keeffe, M., and Yaghi, O.M. (1999) *Nature*, **402**, 276–279.
14. O'Keeffe, M. and Yaghi, O.M. (2012) *Chem. Rev.*, **112**, 675–702.
15. Alexandrov, E.V., Blatov, V.A., Kochetkov, A.V., and Proserpio, D.M. (2011) *CrystEngComm*, **13**, 3947–3958.
16. Yaghi, O.M. and Li, H. (1995) *J. Am. Chem. Soc.*, **117**, 10401–10402.
17. Grzesiak, A.L., Uribe, F.J., Ockwig, N.W., Yaghi, O.M., and Matzger, A.J. (2006) *Angew. Chem. Int. Ed.*, **45**, 2553–2556.
18. Eddaoudi, M., Kim, J., Rosi, N., Vodak, D., Wachter, J., O'Keeffe, M., and Yaghi, O.M. (2002) *Science*, **295**, 469–472.
19. Manos, M.J., Moushi, E.E., Papaefstathiou, G.S., and Tasiopoulos, A.J. (2012) *Cryst. Growth Des.*, **12**, 5471–5480.
20. Kim, D., Liu, X., Oh, M., Song, X., Zou, Y., Singh, D., Kim, K.S., and Lah, M.S. (2014) *CrystEngComm*, **16**, 6391–6397.
21. Wang, Z., Kravtsov, V.C., and Zaworotko, M.J. (2005) *Angew. Chem. Int. Ed.*, **44**, 2877–2880.
22. Lysenko, A.B., Govor, E.V., Krautscheid, H., and Domasevitch, K.V. (2006) *Dalton Trans.*, 3772–3776.
23. Nouar, F., Eubank, J.F., Bousquet, T., Wojtas, L., Zaworotko, M.J., and Eddaoudi, M. (2008) *J. Am. Chem. Soc.*, **130**, 1833–1835.
24. Perry, J.J. IV,, Perman, J.A., and Zaworotko, M.J. (2009) *Chem. Soc. Rev.*, **38**, 1400.
25. (a) Wells, A.F. (1984) *Structural Inorganic Chemistry*, 5th edn, Oxford University Press, Oxford; (b) Van Niekerk, J.N. and Schoening, F.R.L. (1953) *Nature*, **171**, 36–37.
26. Li, H., Eddaoudi, M., Groy, T.L., and Yaghi, O.M. (1998) *J. Am. Chem. Soc.*, **120**, 8571–8572.
27. Chen, B., Eddaoudi, M., Reineke, T.M., Kampf, J.W., O'Keeffe, M., and Yaghi, O.M. (2000) *J. Am. Chem. Soc.*, **122**, 11559–11560.
28. Chui, S.S.Y., Lo, S.M.F., Charmant, J.P.H., Orpen, A.G., and Williams, I.D. (1999) *Science*, **283**, 1148–1150.
29. Delgado-Friedrichs, O., O'Keeffe, M., and Yaghi, O.M. (2006) *Acta Crystallogr., Sect. A*, **62**, 350–355.
30. Millward, A.R. and Yaghi, O.M. (2005) *J. Am. Chem. Soc.*, **127**, 17998–17999.
31. Ma, S., Sun, D., Ambrogio, M., Fillinger, J.A., Parkin, S., and Zhou, H.-C. (2007) *J. Am. Chem. Soc.*, **129**, 1858–1859.
32. Furukawa, H., Go, Y.B., Ko, N., Park, Y.K., Uribe-Romo, F.J., Kim, J., O'Keeffe, M., and Yaghi, O.M. (2011) *Inorg. Chem.*, **50**, 9147–9152.
33. Guo, Z., Wu, H., Srinivas, G., Zhou, Y., Xiang, S., Chen, Z., Yang, Y., Zhou, W., O'Keeffe, M., and Chen, B. (2011) *Angew. Chem. Int. Ed.*, **50**, 3178–3181.
34. Ma, S., Sun, D., Simmons, J.M., Collier, C.D., Yuan, D., and Zhou, H.-C. (2008) *J. Am. Chem. Soc.*, **130**, 1012–1016.
35. Peng, Y., Krungleviciute, V., Eryazici, I., Hupp, J.T., Farha, O.K., and Yildirim, T. (2013) *J. Am. Chem. Soc.*, **135**, 11887–11894.
36. (a) Zhang, Z., Zhang, L., Wojtas, L., Eddaoudi, M., and Zaworotko, M.J. (2011) *J. Am. Chem. Soc.*, **134**, 928–933; (b) Feldblyum, J.I., Liu, M., Gidley, D.W., and Matzger, A.J. (2011) *J. Am. Chem. Soc.*, **133**, 18257–18263; (c) Xie, L., Liu, S., Gao, C., Cao, R., Cao, J., Sun, C., and Su, Z. (2007) *Inorg. Chem.*, **46**, 7782–7788; (d) Maniam, P. and Stock, N. (2011) *Inorg. Chem.*, **50**, 5085–5097.
37. Lee, Y.-G., Moon, H.R., Cheon, Y.E., and Suh, M.P. (2008) *Angew. Chem. Int. Ed.*, **47**, 7741–7745.
38. Chen, B., Ockwig, N.W., Millward, A.R., Contreras, D.S., and Yaghi, O.M. (2005) *Angew. Chem. Int. Ed.*, **44**, 4745–4749.

39. Moulton, B., Lu, J., Hajndl, R., Hariharan, S., and Zaworotko, M.J. (2002) *Angew. Chem. Int. Ed.*, **41**, 2821–2824.
40. Eddaoudi, M., Kim, J., O'Keeffe, M., and Yaghi, O.M. (2002) *J. Am. Chem. Soc.*, **124**, 376–377.
41. (a) Rao, X., Cai, J., Yu, J., He, Y., Wu, C., Zhou, W., Yildirim, T., Chen, B., and Qian, G. (2013) *Chem. Commun.*, **49**, 6719–6721; (b) Lin, X., Jia, J., Zhao, X., Thomas, K.M., Blake, A.J., Walker, G.S., Champness, N.R., Hubberstey, P., and Schröder, M. (2006) *Angew. Chem. Int. Ed.*, **45**, 7358–7364; (c) Perman, J.A., Cairns, A.J., Wojtas, L., Eddaoudi, M., and Zaworotko, M.J. (2011) *CrystEngComm*, **13**, 3130–3133; (d) Gao, W.-Y., Chen, Y., Niu, Y., Williams, K., Cash, L., Perez, P.J., Wojtas, L., Cai, J., Chen, Y.-S., and Ma, S. (2014) *Angew. Chem. Int. Ed.*, **53**, 2615–2619.
42. Li, H., Davis, C.E., Groy, T.L., Kelley, D.G., and Yaghi, O.M. (1998) *J. Am. Chem. Soc.*, **120**, 2186–2187.
43. Clegg, W., Harbron, D.R., Homan, C.D., Hunt, P.A., Little, I.R., and Straughan, B.P. (1991) *Inorg. Chim. Acta*, **186**, 51–60.
44. (a) Tranchemontagne, D., Hunt, J., and Yaghi, O. (2008) *Tetrahedron*, **64**, 8553–8557; (b) Hafizovic, J., Bjørgen, M., Olsbye, U., Dietzel, P.D.C., Bordiga, S., Prestipino, C., Lamberti, C., and Lillerud, K.P. (2007) *J. Am. Chem. Soc.*, **129**, 3612–3620.
45. Zhang, J., Wojtas, L., Larsen, R.W., Eddaoudi, M., and Zaworotko, M.J. (2009) *J. Am. Chem. Soc.*, **131**, 17040–17041.
46. Chae, H.K., Siberio-Perez, D.Y., Kim, J., Go, Y., Eddaoudi, M., Matzger, A.J., O'Keeffe, M., and Yaghi, O.M. (2004) *Nature*, **427**, 523–527.
47. Furukawa, H., Ko, N., Go, Y.B., Aratani, N., Choi, S.B., Choi, E., Yazaydin, A.Ö., Snurr, R.Q., O'Keeffe, M., Kim, J., and Yaghi, O.M. (2010) *Science*, **329**, 424–428.
48. (a) Liu, L., Konstas, K., Hill, M.R., and Telfer, S.G. (2013) *J. Am. Chem. Soc.*, **135**, 17731–17734; (b) Grunker, R., Bon, V., Muller, P., Stoeck, U., Krause, S., Mueller, U., Senkovska, I., and Kaskel, S. (2014) *Chem. Commun.*, **50**, 3450–3452.
49. Deng, H., Doonan, C.J., Furukawa, H., Ferreira, R.B., Towne, J., Knobler, C.B., Wang, B., and Yaghi, O.M. (2010) *Science*, **327**, 846–850.
50. Zhang, Y.-B., Furukawa, H., Ko, N., Nie, W., Park, H.J., Okajima, S., Cordova, K.E., Deng, H., Kim, J., and Yaghi, O.M. (2015) *J. Am. Chem. Soc.*, **137**, 2641–2650.
51. Hou, L., Lin, Y.-Y., and Chen, X.-M. (2008) *Inorg. Chem.*, **47**, 1346–1351.
52. Figgis, B.N. and Robertson, G.B. (1965) *Nature*, **205**, 694–695.
53. Schoedel, A. and Zaworotko, M.J. (2014) *Chem. Sci.*, **5**, 1269–1282.
54. Schnobrich, J.K., Lebel, O., Cychosz, K.A., Dailly, A., Wong-Foy, A.G., and Matzger, A.J. (2010) *J. Am. Chem. Soc.*, **132**, 13941–13948.
55. (a) Cavka, J.H., Jakobsen, S., Olsbye, U., Guillou, N., Lamberti, C., Bordiga, S., and Lillerud, K.P. (2008) *J. Am. Chem. Soc.*, **130**, 13850–13851; (b) Furukawa, H., Gándara, F., Zhang, Y.-B., Jiang, J., Queen, W.L., Hudson, M.R., and Yaghi, O.M. (2014) *J. Am. Chem. Soc.*, **136**, 4369–4381.
56. (a) Gándara, F., Furukawa, H., Lee, S., and Yaghi, O.M. (2014) *J. Am. Chem. Soc.*, **136**, 5271–5274; (b) Ahnfeldt, T., Guillou, N., Gunzelmann, D., Margiolaki, I., Loiseau, T., Férey, G., Senker, J., and Stock, N. (2009) *Angew. Chem. Int. Ed.*, **48**, 5163–5166.
57. Dincă, M., Dailly, A., Liu, Y., Brown, C.M., Neumann, D.A., and Long, J.R. (2006) *J. Am. Chem. Soc.*, **128**, 16876–16883.
58. Dincă, M., Han, W.S., Liu, Y., Dailly, A., Brown, C.M., and Long, J.R. (2007) *Angew. Chem. Int. Ed.*, **46**, 1419–1422.
59. Tan, Y.-X., He, Y.-P., and Zhang, J. (2011) *Chem. Commun.*, **47**, 10647–10649.
60. Jung Soo, S., Dongmok, W., Hyoyoung, L., Sung Im, J., Jinho, O., Young Jin, J., and Kimoon, K. (2000) *Nature*, **404**, 982.
61. (a) Yang, S.Y., Long, L.S., Huang, R.B., and Zheng, L.S. (2002) *Chem. Commun.*, 472–473; (b) Yang, S.Y., Long, L.S., Jiang, Y.B., Huang, R.B., and Zheng, L.S. (2002) *Chem. Mater.*, **14**, 3229–3231.

62. An, J., Farha, O.K., Hupp, J.T., Pohl, E., Yeh, J.I., and Rosi, N.L. (2012) *Nat. Commun.*, **3**, 604.
63. Li, T., Kozlowski, M.T., Doud, E.A., Blakely, M.N., and Rosi, N.L. (2013) *J. Am. Chem. Soc.*, **135**, 11688–11691.
64. Eddaoudi, M., Kim, J., Wachter, J.B., Chae, H.K., O'Keeffe, M., and Yaghi, O.M. (2001) *J. Am. Chem. Soc.*, **123**, 4368–4369.
65. Moulton, B., Lu, J., Mondal, A., and Zaworotko, M.J. (2001) *Chem. Commun.*, 863–864.
66. (a) Furukawa, H., Kim, J., Ockwig, N.W., O'Keeffe, M., and Yaghi, O.M. (2008) *J. Am. Chem. Soc.*, **130**, 11650–11661; (b) Li, J.-R. and Zhou, H.-C. (2010) *Nat. Chem.*, **2**, 893–898.
67. Wang, H.-N., Meng, X., Yang, G.-S., Wang, X.-L., Shao, K.-Z., Su, Z.-M., and Wang, C.-G. (2011) *Chem. Commun.*, **47**, 7128–7130.
68. Perry, J.J., Kravtsov, V.C., McManus, G.J., and Zaworotko, M.J. (2007) *J. Am. Chem. Soc.*, **129**, 10076–10077.
69. Delgado-Friedrichs, O. and O'Keeffe, M. (2007) *Acta Crystallogr., Sect. A*, **63**, 344–347.
70. (a) Luebke, R., Eubank, J.F., Cairns, A.J., Belmabkhout, Y., Wojtas, L., and Eddaoudi, M. (2012) *Chem. Commun.*, **48**, 1455–1457; (b) Zheng, B., Bai, J., Duan, J., Wojtas, L., and Zaworotko, M.J. (2010) *J. Am. Chem. Soc.*, **133**, 748–751; (c) Farha, O.K., Özgür Yazaydın, A., Eryazici, I., Malliakas, C.D., Hauser, B.G., Kanatzidis, M.G., Nguyen, S.T., Snurr, R.Q., and Hupp, J.T. (2010) *Nat. Chem.*, **2**, 944–948; (d) Farha, O.K., Wilmer, C.E., Eryazici, I., Hauser, B.G., Parilla, P.A., O'Neill, K., Sarjeant, A.A., Nguyen, S.T., Snurr, R.Q., and Hupp, J.T. (2012) *J. Am. Chem. Soc.*, **134**, 9860–9863; (e) Yan, Y., Suyetin, M., Bichoutskaia, E., Blake, A.J., Allan, D.R., Barnett, S.A., and Schroder, M. (2013) *Chem. Sci.*, **4**, 1731–1736; (f) Yuan, D., Zhao, D., Sun, D., and Zhou, H.-C. (2010) *Angew. Chem. Int. Ed.*, **49**, 5357–5361; (g) Hong, S., Oh, M., Park, M., Yoon, J.W., Chang, J.-S., and Lah, M.S. (2009) *Chem. Commun.*, 5397–5399; (h) Li, B., Zhang, Z., Li, Y., Yao, K., Zhu, Y., Deng, Z., Yang, F., Zhou, X., Li, G., Wu, H., Nijem, N., Chabal, Y.J., Lai, Z., Han, Y., Shi, Z., Feng, S., and Li, J. (2012) *Angew. Chem. Int. Ed.*, **51**, 1412–1415.
71. Eubank, J.F., Nouar, F., Luebke, R., Cairns, A.J., Wojtas, L., Alkordi, M., Bousquet, T., Hight, M.R., Eckert, J., Embs, J.P., Georgiev, P.A., and Eddaoudi, M. (2012) *Angew. Chem. Int. Ed.*, **51**, 10099–10103.
72. Farha, O.K., Eryazici, I., Jeong, N.C., Hauser, B.G., Wilmer, C.E., Sarjeant, A.A., Snurr, R.Q., Nguyen, S.T., Yazaydın, A.Ö., and Hupp, J.T. (2012) *J. Am. Chem. Soc.*, **134**, 15016–15021.
73. Li, J.-R., Timmons, D.J., and Zhou, H.-C. (2009) *J. Am. Chem. Soc.*, **131**, 6368–6369.
74. Stoeck, U., Krause, S., Bon, V., Senkovska, I., and Kaskel, S. (2012) *Chem. Commun.*, **48**, 10841–10843.
75. Stoeck, U., Senkovska, I., Bon, V., Krause, S., and Kaskel, S. (2015) *Chem. Commun.*, **51**, 1046–1049.
76. Rosi, N.L., Kim, J., Eddaoudi, M., Chen, B., O'Keeffe, M., and Yaghi, O.M. (2005) *J. Am. Chem. Soc.*, **127**, 1504–1518.
77. Deng, H., Grunder, S., Cordova, K.E., Valente, C., Furukawa, H., Hmadeh, M., Gándara, F., Whalley, A.C., Liu, Z., Asahina, S., Kazumori, H., O'Keeffe, M., Terasaki, O., Stoddart, J.F., and Yaghi, O.M. (2012) *Science*, **336**, 1018–1023.
78. (a) McDonald, T.M., Lee, W.R., Mason, J.A., Wiers, B.M., Hong, C.S., and Long, J.R. (2012) *J. Am. Chem. Soc.*, **134**, 7056–7065; (b) Fracaroli, A.M., Furukawa, H., Suzuki, M., Dodd, M., Okajima, S., Gándara, F., Reimer, J.A., and Yaghi, O.M. (2014) *J. Am. Chem. Soc.*, **136**, 8863–8866.
79. Queen, W.L., Bloch, E.D., Brown, C.M., Hudson, M.R., Mason, J.A., Murray, L.J., Ramirez-Cuesta, A.J., Peterson, V.K., and Long, J.R. (2012) *Dalton Trans.*, **41**, 4180–4187.
80. Bloch, E.D., Queen, W.L., Krishna, R., Zadrozny, J.M., Brown, C.M., and Long, J.R. (2012) *Science*, **335**, 1606–1610.
81. An, J., Geib, S.J., and Rosi, N.L. (2009) *J. Am. Chem. Soc.*, **131**, 8376–8377.
82. An, J., Geib, S.J., and Rosi, N.L. (2009) *J. Am. Chem. Soc.*, **132**, 38–39.